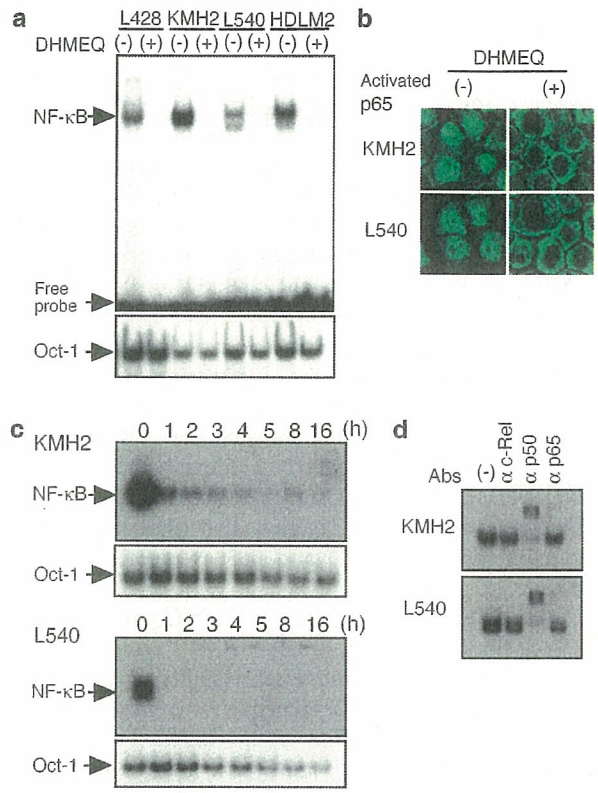


**Figure 3** DHMEQ suppresses constitutive NF-κB activity in H-RS cell lines. (**a**) Inhibition of constitutive NF-κB-binding activity in H-RS cell lines. H-RS cell lines, L428, KMH2, L540 and HDLM2, were treated with (+) or without (−) 10 μg/ml of DHMEQ for 7 h. Nuclear extracts (2 μg) were examined for NF-κB binding activity by EMSA with a radiolabeled NF-κB specific probe. The upper panel shows inhibition of NF-κB-binding activity by DHMEQ. The lower panel shows results of EMSA with a control probe, Oct-1. The position of shifted bands corresponding to NF-κB and free probes are indicated on the left. (**b**) Accumulation of active NF-κB p65 in the cytoplasm after DHMEQ treatment. KMH2 and L540 cells were treated with or without 10 μg/ml of DHMEQ for 6 h. Confocal immunofluorescence microscopic analysis was carried out on cytospin samples stained with antibody against active NF-κB p65. (**c**) Time-course studies of NF-κB inhibition by DHMEQ. KMH2 and L540 cells were treated with 10 μg/ml of DHMEQ for indicated hours. Nuclear extracts (2 μg) were examined for NF-κB-binding activity by EMSA with a radiolabeled NF-κB-specific probe. EMSA with Oct-1 served as control. (**d**) NF-κB subcomponent analysis in H-RS cell lines. Subcomponents of NF-κB constitutively activated in H-RS cell lines were determined by supershift analysis. Nuclear extracts (2 μg) of untreated H-RS cell lines were subjected to supershift analysis with antibodies specific for c-Rel, NF-κB p50 and NF-κB p65. Cell lines used are indicated on the left.

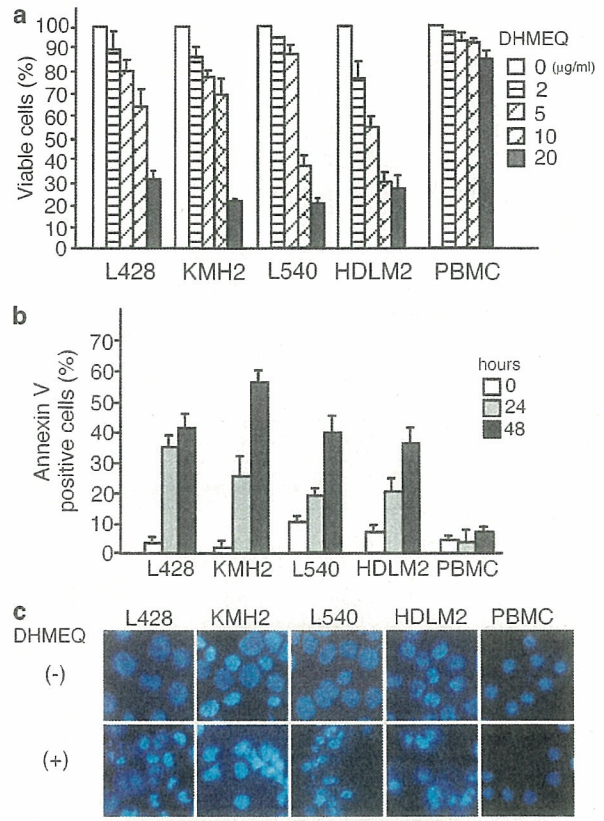


**Figure 4** DHMEQ induces apoptosis of H-RS cell lines. (**a**) Dose-dependent reduction of cell viabilities of H-RS cell lines treated with DHMEQ. H-RS cell lines; L428, KMH2, L540 and HDLM2 as well as PBMC were treated with indicated concentrations of DHMEQ for 48 h. Cell viabilities were determined by MTT assay. Data represent the mean ± s.d. of three independent experiments. (**b**) Flow cytometric analysis of Annexin V-reactive cells. L428 and KMH2 cells were treated with 20 μg/ml of DHMEQ for indicated hours. L540 and HDLM2 cells were treated with 10 μg/ml of DHMEQ. PBMC were treated with 20 μg/ml of DHMEQ. After labeling with FITC-conjugated Annexin V, cells were analyzed by flow cytometry. Data represent the mean ± s.d. of three independent experiments. (**c**) Nuclear fragmentation of cells treated with DHMEQ. Cells were treated with the same concentration of DHMEQ used in the detection of Annexin V reactive cells for 48 h and stained with 10 μM Hoechst 33342. Cells used are indicated above.

second and third panels). To confirm this, we next studied whether inhibitors of caspase 3, 8 and 9 can inhibit DHMEQ-induced apoptosis. The results demonstrated significant alleviation of apoptosis in the cells treated by these inhibitors, although inhibition of apoptosis was not complete (Figure 5b). These results suggested that the apoptosis induced by DHMEQ is mediated by both membranous and mitochondrial caspase pathways.

Recent reports indicate frequent expression of anti-apoptotic genes Bcl-xL and c-FLIP whose constitutive induction are critically involved in anti-apoptotic activity in H-RS cells.[21–24] Bcl-xL and c-FLIP antagonize mitochondrial and membranous caspase activities.[25] We next examined changes in their expression upon DHMEQ treatment by Northern blotting and immunohistochemistry. The result confirmed downregulation of Bcl-xL and c-FLIP mRNAs (Figure 5c). We also examined the protein expression of Bcl-xL and c-FLIP by immunofluorescence confocal microscopy. The results clearly showed downregulation of expression of these proteins (Figure 5d). Taken together, these data confirmed that DHMEQ induced apoptosis of H-RS cell lines is

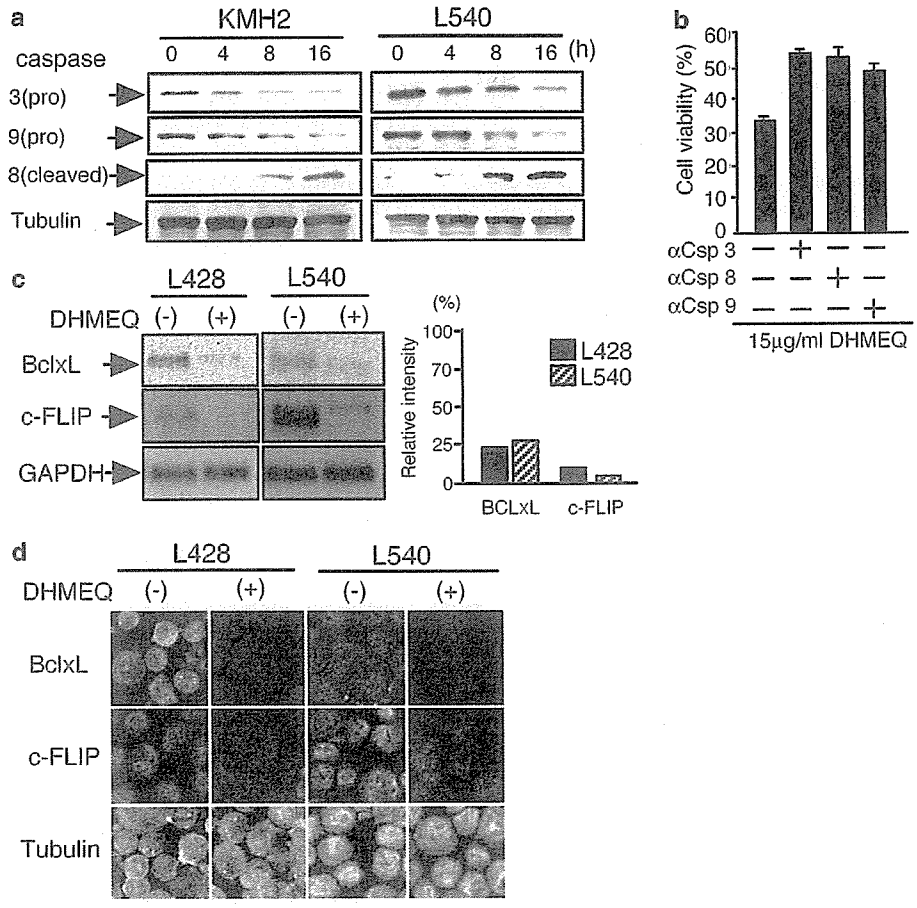


**Figure 5** DHMEQ-induced apoptosis of H-RS cell lines involves activation of membranous and mitochondrial caspase pathways and downregulation of c-FLIP and Bcl-xL. (**a**) Immunoblot analyses of caspase -3, -8 and -9. L540 cells were treated with 10 μg/ml of DHMEQ and KMH2 cells were treated of 20 μg/ml with DHMEQ for indicated hours. 30 μg of whole cell lysates were subjected to the analysis. (**b**) Inhibition of DHMEQ induced apoptosis by blockade of caspase-3, -8 and -9 activities in KMH2 cells. Before the incubation with 15 μg/ml of DHMEQ, KMH2 cells were treated with 50 μM of caspase 3 inhibitor z-DEVD-FMK, caspase 8 inhibitor z-IETD-FMK or caspase 9 inhibitor z-LEHD-FMK. After 12 h of treatment with DHMEQ, cells were analyzed by MTT assay. α-Csp, anti-caspase. (**c**) The expression of Bcl-xL and c-FLIP mRNA. L428 and L540 cells were treated with or without 10 μg/ml of DHMEQ for 16 h. The expression of Bcl-xL and c-FLIP was examined by Northern blot analysis, using RT-PCR amplified fragments as probes. Two microgramof poly (A)-selected RNA were subjected to the analysis. Results of Northern blot analyses are shown on the left. Expression of GAPDH served as a control. Quantification of relative levels of expression is shown on the right. GAPDH signals were measured by densitometry and the values were used to normalize the levels of densitometric quantification of Bcl-xL and c-FLIP mRNA expression in L428 and L540 cells. The relative expression levels of treated samples are expressed as percentages of those of untreated ones, which are set to 100%. (**d**) Expression of Bcl-xL and c-FLIP proteins involved in anti-apoptosis. L428 and L540 cells were treated with or without 10 μg/ml of DHMEQ for 16 h. Cells were spun by centrifugation onto glass coverslips and stained with antibodies specific for Bcl-xL and c-FLIP and observed with fluorescence confocal microscopy. Expression of α-tubulin served as control.

mediated via mitochondrial and membranous pathway, which are accompanied by downregulation of Bcl-xL and c-FLIP.

### DHMEQ Shows a Potent Inhibitory Effect on the Growth of H-RS Cells in NOG Mice Model

As the above results suggested potential efficacy of DHMEQ for the treatment of patients with HL by inhibiting constitutive NF-κB activity, we next examined whether DHMEQ treatment can suppress growth of xenografted H-RS cells in the NOG mice model. As expected, DHMEQ treatment resulted in reduction of the tumor mass at 1 month after inoculation (Figure 6a). A significant decrease in the size and weight of tumors in mice treated with DHMEQ was demonstrated when compared with controls at 1 month (Figure 6b). DHMEQ also inhibited the size and growth of tumors established by inoculation of L540 and KMH2 cells, indicating that the action of DHMEQ is independent of lack of wild-type IκBα as is expected by experiments *in vitro* (Figure 6c and d). DHMEQ at this treatment dosage (12 mg/kg of DHMEQ, three times a week for 1 month) is well tolerated without adverse findings such as weight loss or cachexia of treated mice. As expected, microscopic analysis of tumors revealed apoptotic cells in specimens from

DHMEQ-treated mice (Figure 6e). These results suggest that DHMEQ contributes to the reduction of HL tumors independent of lack of IκBα in mice model.

### DHMEQ Enhances Anti-Tumor Effect of Topoisomerase Inhibitors by Blocking Inducible NF-κB in H-RS Cells

We next examined the effects of DHMEQ on NF-κB activity induced by topoisomerase inhibitors in KMH2 cells. Treatment by DHMEQ almost completely abrogated both constitutive and inducible NF-κB activities (Figure 7a). Analysis by confocal microscopy revealed accumulation of active form of NF-κB p65 in the cytoplasm of KMH2 cells treated with SN-38 and DHMEQ, supporting the notion that DHMEQ inhibits these NF-κB at the level of translocation into the nucleus (Figure 7b).

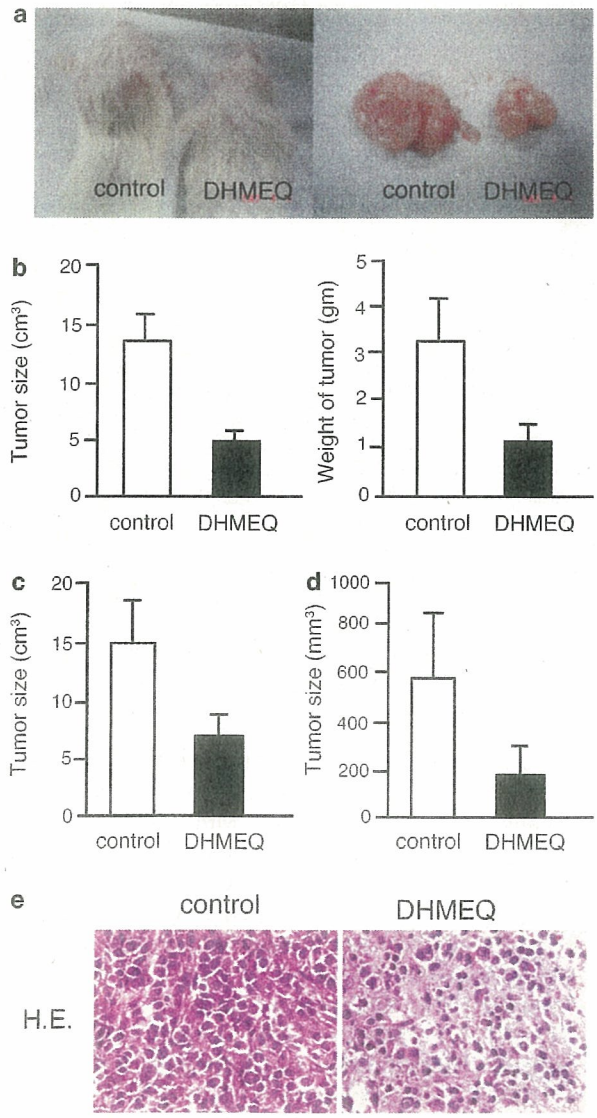


We next examined whether topoisomerase inhibitors and DHMEQ show enhanced anti-tumor effects in H-RS cell lines. We incubated KMH2 cells with sublethal concentrations of SN-38 with or without 10 μg/ml of DHMEQ for 48 h. The viability of the cells was measured by MTT assay. Combination of DHMEQ and SN-38 showed enhanced effect in the reduction of cell viability of KMH2 cells (Figure 7c left panel). Other topoisomerase inhibitors, daunorubicin and etoposide also revealed almost the same effects (Figure 7c middle and right panel).

To explore whether the combined effects result in enhanced induction of apoptosis, we examined expression of Annexin V, a marker for the early stage of apoptosis, and nuclear fragmentation of KMH2 cells. In each combination with one of three topoisomerase inhibitors, DHMEQ treatment enhanced Annexin V staining (Figure 7d) and fragmentation or condensation of the nuclei (Figure 7e). DHMEQ also enhanced SN-38-induced activation of caspase 3 in L428 cells (Figure 7f). These observations indicate that blockade of inducible NF-κB by DHMEQ enhances the anti-tumor effects of topoisomerase inhibitors in H-RS cells.

## DISCUSSION

In this study, we showed that although the NF-κB level of H-RS cell is very high, topoisomerase inhibitors further stimulated NF-κB activity through IKK activation in not only H-RS cell lines with wild-type IκBα, but also H-RS cell lines with defective IκBα. We presented the supportive evidence that IκBβ is involved in NF-κB induction in H-RS cells. We also showed that a new NF-κB inhibitor, DHMEQ-enhanced cytotoxicity of topoisomerase inhibitors by inhibiting inducible NF-κB, independent of the presence or absence of IκBα mutations in H-RS cell lines. The results suggest that constitutive and inducible NF-κB are appropriate molecular targets for the treatment of HL, and DHMEQ is a suitable compound to target these NF-κB.

**Figure 6** Effects of DHMEQ on H-RS cell lines inoculated in NOG mice. A total of $1 \times 10^7$ cells were inoculated in the post-auricular region of NOG mice. For the treatment group, 12 mg/kg of DHMEQ was administered intraperitoneally three times a week for 1 month, beginning on either day 0 or day 5 when tumors were palpable and established. The control mice received RPMI 1640 (200 μl) simultaneously. (**a**) Gross appearance of the mice with (right) or without (left) DHMEQ treatment. Macroscopic images of subcutaneous tumors formed by L540 and those resected from mice with (right) or without (left) DHMEQ treatment, which began on day 0. (**b**) Size and weight of the resected tumors were measured and represented as bar graphs. Data represent the mean ± s.d. from six mice. (**c** and **d**) Effects of DHMEQ on established tumors. L540 cells (**c**) and KMH2 cells (**d**) were used for the experiments. Size of tumors was measured and represented as bar graphs. Data represent the mean ± s.d. from four mice. (**e**) Growth inhibitory effect of DHMEQ on L540 cells is accompanied by apoptosis. Microscopic images of HE-stained tumor tissues of mice with or without DHMEQ treatment (right and left, respectively) revealed apoptotic cells in DHMEQ-treated mice.

Activation of IKK and IκBα upon NF-κB induction by topoisomerase inhibitors has been well-documented.[12,14] Topoisomerase inhibitors are thought to mobilize a pre-existing signaling pathway that starts from the nucleus at the level of DNA strand breaks to end up in the cytosol at the IKK complex. Several candidate molecules such as ATM

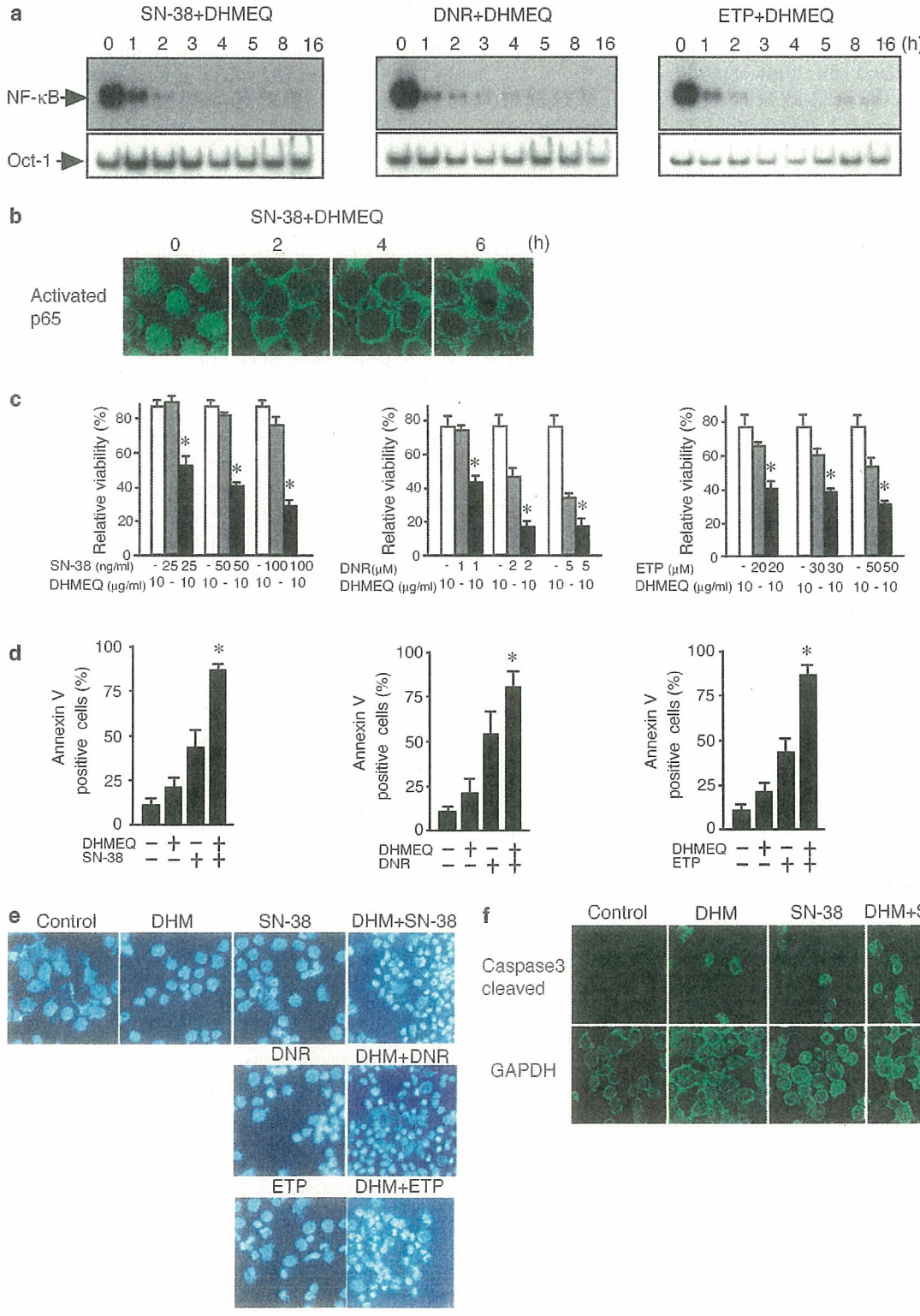

and DNA-PK involved in this step have been reported.[26,27] A previous study excluded involvement of an autocrine NF-κB activator synthesized by stimulation of topoisomerase inhibitors.[12] Transient activation of IKK and NF-κB by topoisomerase inhibitors in H-RS cell lines indicates that similar kind of activation pathway also operates in H-RS cells having strong and constitutive NF-κB activity.

About 10–20% of H-RS cells are reported to harbor hetero- or homo-genetic alteration of IκBα genes resulting in the production of defective IκBα lacking C-terminal domain unable to bind with NF-κB. Lack of wild-type IκBα by IκBα mutations has been reported to one of the causes of constitutive NF-κB activation in H-RS cells.[3–7] If IκBα is the only molecule that regulates NF-κB in H-RS cells, lack of wild-type IκBα may cause deregulated activation of NF-κB independent of upstream IKK signals. However, IKK-mediated induction of NF-κB by topoisomerase inhibitors in H-RS cell lines lacking wild-type IκBα suggests the existence of other molecules that regulate NF-κB activity by substitution for IκBα. Our previous result that adenovirus-mediated transduction of decoy CD30 lacking the cytoplasmic domain inhibits NF-κB activity and the recent report that proteasome inhibitor PS341 induces apoptosis in H-RS cell lines lacking wild-type IκBα, support the above hypothesis.[8,28] The results in this study indicate that IκBβ is involved in NF-κB activation in H-RS cells and IκBβ substitutes for IκBα in H-RS cells lacking wild-type IκBα. Functional redundancy and similar kinetics of activities of IκBα and IκBβ reported previously also support the above notion.[19]

The results obtained in this study suggest that not only constitutive, but also inducible NF-κB activities are good molecular targets of HL treatment. The results confirmed that topoisomerase inhibitors, SN-38, daunorubicin and etoposide can further induce transient NF-κB activation in addition to the basal strong and constitutive NF-κB activity in H-RS cell lines. Previous studies showed that stimulation of H-RS cell lines by TNF family members; CD40L or TNF cannot enhance NF-κB activity.[5,6] These observations indicate that in H-RS cells, signals from TNF receptor family members to IKK complex, which are mediated by TRAF proteins, are fully active, whereas IKK complex is still responsible for TRAF-independent stimulation. The demonstration that DHMEQ enhanced effects of topoisomerase inhibitors by blocking inducible NF-κB, suggests that inducible NF-κB blunts the effects of topoisomerase inhibitors in H-RS cells and DHMEQ can restore this effect.

Blockade of NF-κB is evident at 1 h and thereafter (Figure 3c), apoptosis induction was at a relatively late event after DHMEQ treatment (Figure 4b). Therefore, induction of apoptosis in H-RS cells by DHMEQ may be indirect and mediated by altered levels of gene expression. As inhibition of constitutive NF-κB activation is sufficient to trigger apoptosis of H-RS cells without stimulation of death receptor or cytotoxic agents, survival of H-RS cells appears to depend on a balance between anti-apoptotic and pro-apoptotic activities. In support of this notion, the present study confirmed the downregulation of c-FLIP and Bcl-xL, which are reported to be frequently expressed in H-RS cells upon blocking of NF-κB activity[21–24] (Figure 5c and d).

Prompt and specific action of DHMEQ suggests that DHMEQ is a suitable compound to target NF-κB in H-RS cells. Recent studies in other laboratories using gliotoxin, MG132, arcenic and PS341 also suggest that low-molecular-weight compounds have a potential to inhibit NF-κB in H-RS cells. However, their specificity for the NF-κB pathway appears to be relatively low when compared with that of DHMEQ.[28–30] The target of DHMEQ resides downstream of targets of gliotoxin, MG132, arcenic and PS341. Furthermore, inhibition of NF-κB by gliotoxin, MG132, and PS341 is only one of the results of their activities as proteasome inhibitors.[28,29] Arsenic also alters a variety of enzymatic activities because of reactivity with sulfhydryl groups.[30]

The unique properties of DHMEQ appear to minimize adverse effects on normal cells. Notably, PBMC are resistant to apoptosis by DHMEQ treatment, although the mechanism is not currently understood. Results of our *in vivo* model suggest that DHMEQ may be minimally less toxic at effective doses. Treatment of mice with DHMEQ three times a week

**Figure 7** DHMEQ abrogates inducible NF-κB and enhances anti-tumor effect of topoisomerase inhibitors in H-RS cell lines. (**a**) Inhibition of topoisomerase inhibitors-mediated NF-κB induction by DHMEQ. KMH2 cells were exposed to 100 ng/ml of SN-38, 2 μM daunorubicin or 50 μM etoposide in combination with 10 μg/ml of DHMEQ for indicated hours. Two microgram of nuclear extracts were examined for NF-κB-binding activity by EMSA using NF-κB probe. Lower panels show results of EMSA with a control probe, Oct-1. DNR, daunorubicin; ETP, etoposide. (**b**) Accumulation of active NF-κB p65 after DHMEQ treatment. KMH2 cells were exposed to 100 ng/ml of SN-38 in combination with 10 μg/ml of DHMEQ for indicated hours. Confocal immunofluorescence microscopic analysis was carried out on cytospin samples stained with antibody against active NF-κB p65. (**c**) Effect of DHMEQ on viability of H-RS cells treated by topoisomerase inhibitors. KMH2 cells were treated with indicated concentrations of topoisomerase inhibitors with or without 10 μg/ml of DHMEQ. Forty-eight hours after treatment, cell viability was measured by MTT assay and the relative viability was determined. MTT values of DMSO-treated cells were set to 100%. Data present the mean ± s.d. of three independent experiments. $^*P<0.05$, compared with SN-38, DNR or ETP alone. (**d**) Analysis of Annexin V-reactive cells. KMH2 cells were treated with 10 μg/ml of DHMEQ with or without topoisomerase inhibitors for 24 h. Cells were stained by FITC-conjugated Annexin V and analyzed by flow cytometry. Data present the mean ± s.d. of three independent experiments. Concentration of the agents was SN-38; 100 ng/ml, daunorubicine; 2 μM and etoposide; 50 μM. $^*P<0.05$, compared with SN-38, DNR or ETP alone. (**e**) Nuclear fragmentation. KMH2 cells were treated with topoisomerase inhibitors with or without 10 μg/ml of DHMEQ for 24 h. After treatment, KMH2 cells were harvested and subjected to staining by Hoechst 33342. Concentration of the agents was the same as in flow cytometric analysis of Annexin V-reactive cells DHM, DHMEQ. (**f**) Activation of caspase-3. L428 cells were treated with 100 ng/ml of SN-38 with or without 10 μg/ml of DHMEQ for 24 h. Cells were spun onto slide glass and stained with antibody for cleaved caspase-3 and analyzed by confocal microscopy. Staining by GAPDH served as a control.

showed significant anti-tumor activity. DHMEQ treatment did not show significant systemic toxicity such as body weight loss in these experiments. The dose of DHMEQ used in these experiments (12 mg/kg) is far less than LD50 of DHMEQ that is 180 mg/kg (unpublished observation). Therefore, DHMEQ may be more suitable for NF-κB inhibition in H-RS cells.

In conclusion, both constitutive and inducible NF-κB are potential molecular targets to treat HL independent of the presence of IκBα mutations. NF-κB inhibitor DHMEQ is a suitable candidate to translate this strategy into clinical medicine. The results also indicate that IκBβ is involved in NF-κB activation in H-RS cells and IκBβ substitutes for IκBα in H-RS cells lacking wild-type IκBα.

ACKNOWLEDGEMENT

We thank Y Sato, National Institute of Infectious Diseases for technical assistance. Supported in part by Grants-in-Aid for Scientific Research from Japanese Society for Promotion of Science to R Horie and T Watanabe and Integrative Research Program of the Graduate School of Medical Sciences, Kitasato University to R Horie. Also supported in part by grants from the Ministry of Education, Science and Culture, Ministry of Health, Labor and Welfare and Human Health Science of Japan to N Yamamoto. Dr Kadin is supported by NIH Grant P50-CA-93683-05.

1. Diehl V, Thomas RK, Re D. Part II: Hodgkin's lymphoma—diagnosis and treatment. Lancet Oncol 2004;5:19–26.
2. Griffin J. The biology of signal transduction inhibition: basic science to novel therapies. Semin Oncol 2001;28:3–8.
3. Emmerich F, Meiser M, Hummel M, *et al.* Overexpression of I kappa B alpha without inhibition of NF-kappaB activity and mutations in the I kappa B alpha gene in Reed-Sternberg cells. Blood 1999;94:3129–3134.
4. Jungnickel B, Staratschek-Jox A, Brauninger A, *et al.* Clonal deleterious mutations in the IkappaBalpha gene in the malignant cells in Hodgkin's lymphoma. J Exp Med 2000;191:395–402.
5. Krappmann D, Emmerich F, Kordes U, *et al.* Molecular mechanisms of constitutive NF-kappaB/Rel activation in Hodgkin/Reed-Sternberg cells. Oncogene 1999;18:943–953.
6. Wood KM, Roff M, Hay RT. Defective IkappaBalpha in Hodgkin cell lines with constitutively active NF-kappaB. Oncogene 1998;16:2131–2139.
7. Cabannes E, Khan G, Aillet F, *et al.* Mutations in the IkBa gene in Hodgkin's disease suggest a tumour suppressor role for IkappaBalpha. Oncogene 1999;18:3063–3070.
8. Horie R, Watanabe T, Morishita Y, *et al.* Ligand-independent signaling by overexpressed CD30 drives NF-kappaB activation in Hodgkin/Reed-Sternberg cells. Oncogene 2002;21:2493–2503.
9. Bargou RC, Leng C, Krappmann D, *et al.* High-level nuclear NF-kappa B and Oct-2 is a common feature of cultured Hodgkin/Reed-Sternberg cells. Blood 1996;87:4340–4347.
10. Bargou RC, Emmerich F, Krappmann D, *et al.* Constitutive nuclear factor-kappaB-RelA activation is required for proliferation and survival of Hodgkin's disease tumor cells. J Clin Invest 1997;100:2961–2969.
11. Mayo MW, Baldwin AS. The transcription factor NF-kappaB: control of oncogenesis and cancer therapy resistance. Biochim Biophys Acta 2000;1470:M55–M62.
12. Bottero V, Busuttil V, Loubat A, *et al.* Activation of nuclear factor kappaB through the IKK complex by the topoisomerase poisons SN38 and doxorubicin: a brake to apoptosis in HeLa human carcinoma cells. Cancer Res 2001;61:7785–7791.
13. Wang CY, Cusack Jr JC, Liu R, *et al.* Control of inducible chemoresistance: enhanced anti-tumor therapy through increased apoptosis by inhibition of NF-kappaB. Nat Med 1999;5:412–417.
14. Cusack Jr JC, Liu R, Houston M, *et al.* Enhanced chemosensitivity to CPT-11 with proteasome inhibitor PS-341: implications for systemic nuclear factor-kappaB inhibition. Cancer Res 2001;61: 3535–3540.
15. Ariga A, Namekawa J, Matsumoto N, *et al.* Inhibition of tumor necrosis factor-alpha -induced nuclear translocation and activation of NF-kappa B by dehydroxymethylepoxyquinomicin. J Biol Chem 2002;277: 24625–24630.
16. Matsumoto N, Ariga A, To-e S, *et al.* Synthesis of NF-kappaB activation inhibitors derived from epoxyquinomicin C. Bioorg Med Chem Lett 2000;10:865–869.
17. Horie R, Watanabe M, Ishida T, *et al.* The NPM-ALK oncoprotein abrogates CD30 signaling and constitutive NF-kappaB activation in anaplastic large cell lymphoma. Cancer Cell 2004;5:353–364.
18. Dewan MZ, Watanabe M, Terashima K, *et al.* Prompt tumor formation and maintenance of constitutive NF-kappaB activity of multiple myeloma cells in NOD/SCID/gammacnull mice. Cancer Sci 2004;95:564–568.
19. Cheng JD, Ryseck RP, Attar RM, *et al.* Functional redundancy of the nuclear factor kappa B inhibitors I kappa B alpha and I kappa B beta. J Exp Med 1998;188:1055–1062.
20. Huang TT, Miyamoto S. Postrepression activation of NF-kappaB requires the amino-terminal nuclear export signal specific to IkappaBalpha. Mol Cell Biol 2001;21:4737–4747.
21. Kim LH, Nadarajah VS, Peh SC, *et al.* Expression of Bcl-2 family members and presence of Epstein-Barr virus in the regulation of cell growth and death in classical Hodgkin's lymphoma. Histopathology 2004;44:257–267.
22. Dutton A, O'Neil JD, Milner AE, *et al.* Expression of the cellular FLICE-inhibitory protein (c-FLIP) protects Hodgkin's lymphoma cells from autonomous Fas-mediated death. Proc Natl Acad Sci USA 2004;101:6611–6616.
23. Thomas RK, Kallenborn A, Wickenhauser C, *et al.* Constitutive expression of c-FLIP in Hodgkin and Reed-Sternberg cells. Am J Pathol 2002;160:1521–1528.
24. Mathas S, Lietz A, Anagnostopoulos I, *et al.* c-FLIP mediates resistance of Hodgkin/Reed-Sternberg cells to death receptor-induced apoptosis. J Exp Med 2004;199:1041–1052.
25. Debatin KM. Apoptosis pathways in cancer and cancer therapy. Cancer Immunol Immunother 2004;53:153–159.
26. Piret B, Schoonbroodt S, Piette J. The ATM protein is required for sustained activation of NF-kappaB following DNA damage. Oncogene 1999;18:2261–2271.
27. Basu S, Rosenzweig KR, Youmell M, *et al.* The DNA-dependent protein kinase participates in the activation of NF kappa B following DNA damage. Biochem Biophys Res Commun 1998;247:79–83.
28. Zheng B, Georgakis GV, Li Y, *et al.* Induction of cell cycle arrest and apoptosis by the proteasome inhibitor PS-341 in Hodgkin disease cell lines is independent of inhibitor of nuclear factor-kappaB mutations or activation of the CD30, CD40, and RANK receptors. Clin Cancer Res 2004;10:3207–3215.
29. Izban KF, Ergin M, Huang Q, *et al.* Characterization of NF-kappaB expression in Hodgkin's disease: inhibition of constitutively expressed NF-kappaB results in spontaneous caspase-independent apoptosis in Hodgkin and Reed-Sternberg cells. Mod Pathol 2001;14: 297–310.
30. Mathas S, Lietz A, Janz M, *et al.* Inhibition of NF-kappaB essentially contributes to arsenic-induced apoptosis. Blood 2003;102:1028–1034.

Retrovirology

BioMed Central

Short report

Open Access

# 5' long terminal repeat (LTR)-selective methylation of latently infected HIV-1 provirus that is demethylated by reactivation signals

Takaomi Ishida, Akiko Hamano, Tsukasa Koiwa and Toshiki Watanabe*

Address: Laboratory of Tumor Cell Biology, Department of Medical Genome Sciences, Graduate School of Frontier Sciences, The University of Tokyo, 4-6-1 Shirokanedai, Minato-ku, Tokyo 108–8639, Japan

Email: Takaomi Ishida - tishida@ims.u-tokyo.ac.jp; Akiko Hamano - ahamano@mbox.co.jp; Tsukasa Koiwa - koiwa@mac.com; Toshiki Watanabe* - tnabe@ims.u-tokyo.ac.jp

* Corresponding author

Published: 12 October 2006

*Retrovirology* 2006, **3**:69 doi:10.1186/1742-4690-3-69

Received: 15 November 2005
Accepted: 12 October 2006

This article is available from: http://www.retrovirology.com/content/3/1/69

© 2006 Ishida et al; licensee BioMed Central Ltd.
This is an Open Access article distributed under the terms of the Creative Commons Attribution License (http://creativecommons.org/licenses/by/2.0), which permits unrestricted use, distribution, and reproduction in any medium, provided the original work is properly cited.

## Abstract

We previously described selective hypermethylation of the 5'-long terminal repeat (LTR) of HTLV-I provirus *in vivo* and *in vitro*. This prompted us to analyze CpG methylation of the two LTRs of the HIV provirus in chronically infected cell lines. The results demonstrate selective hypermethylation of the 5' LTR of the HIV provirus in ACH-2 cells. Moreover, induction of viral gene expression by TNF-α resulted in demethylation of the 5'-LTR. These results suggest that selective epigenetic modification of the 5'LTR of the HIV-1 provirus may be an important mechanism by which proviral activity is suppressed.

## Findings

With the use of highly active anti-retroviral therapy (HAART) for HIV-infected individuals, greater control of viral replication is now possible. The widespread use of HAART has led to a substantial decline in the incidence of acquired immunodeficiency syndrome (AIDS) and AIDS-related mortality [1-6]. This development has led to considerable optimism [7], but complete eradication of HIV from an infected individual is difficult to achieve because there are latently infected resting CD4+ T cells carrying replication-competent HIV resistant to HAART [8-11]. A better understanding of mechanisms underlying latency and reactivation of HIV might yield information on how to overcome the resistance of latent HIV to treatment, and this would contribute to the goal of containment or purging of HIV.

Epigenetic control is thought to be involved in latent infection of HIV. Epigenetic mechanisms result in the heritable silencing of genes without a change in their coding sequence. Three systems, including DNA methylation, RNA-associated silencing and histone modification, are used to initiate and sustain epigenetic silencing [12]. Histone deacetylation is important for quiescence of HIV gene expression in infected resting CD4+ T lymphocytes. Blockade of histone deacetylase (HDAC) activity can stimulate the release of virus from latently infected CD4+ T-cells in vitro and, in combination with enfuvirtde, reduces the pool of CD4+ T-cells *in vivo*[13-15].

CpG methylation has been implicated in silencing of the integrated provirus genome [16,17] as well as in regulation of many imprinted genes [18]. Demethylation induced by an inhibitor of DNA methyltransferase, 5-Aza-cytidine (5-AzaC), was shown to reactivate a latent provirus [19]. *In vitro* studies have shown that DNA methylation suppresses the promoter activity of the HIV-1 long terminal repeat (LTR) [20-23], suggesting that CpG methylation may play an important role in viral latency *in vivo*.

Cytokines such as TNF-α induce HIV gene expression in chronically infected T cell lines [24,25], as well as in latently infected lymphocytes *in vivo* [26,27]. Using chronically infected T cell lines, we investigated CpG methylation of provirus LTR and its relationship to regulatory mechanisms that reactivate the latent HIV provirus. We found that CpG sites in the 5'-LTR are selectively hypermethylated, and that TNF-α-induced reactivation is associated with demethylation of the 5' LTR. Our observations provide clues to the mechanism of signal-mediated demethylation and reactivation of latent HIV.

To evaluate the effects of CpG methylation on the promoter activity of the HIV LTR, we first tested the effects of *in vitro* CpG methylation of HIV LTR-luciferase constructs on activity in transient transfection assays. When transfected into Jurkat cells, the HIV LTR-Luc plasmid showed significant basal levels of luciferase activities, whereas SssI methylase-treated HIV LTR-Luc plasmid showed 100-fold lower luciferase activities (Fig. 1A). We also found that CpG methylation suppressed the LTR's response to activating agents such as HIV Tat or TNF-α. The small responses we observed might be due to incomplete methylation of CpG during SssI methylase treatment, since bisulfite-sequencing analysis of the SssI-treated plasmid detected some unmethylated copies (data not shown). Thus, CpG methylation of the HIV LTR suppresses both basal promoter activity and responses to activating stimuli; this confirms results of earlier studies [20-23].

We next asked if LTRs of integrated proviruses were methylated. Using bisulfite genomic sequencing [28], we analyzed methylation of each CpG site in the U3 region of the HIV-1 LTR in chronically infected cell lines. Primers used for amplification of the modified sense strand are: LTR forward primer (F-3): 5'-TTTGTTATATTTTGTGAGTTTG-TAT-3' (nucleotide position: 200 to 224, 9285 to 9309), reverse primer (R-1), 5'-CAAAAAACTCCCAAACT-CAAATCTA-3' (nucleotide position: 496 to 472, 9581 to 9557). Amplified products were cloned by the TA method followed by sequence analysis using an automated sequencer (Amersham Bioscience, Gene Rapid). The results showed various levels of CpG methylation in Molt 20-2, ACH-2 and U-1 cell lines, which correlated inversely with basal levels of viral gene expression (Fig. 1B and C).

We then asked if TNF-α-induced HIV-1 gene expression in ACH-2 is associated with changes in CpG methylation in the LTR. TNF-α stimulation induced activation of viral gene expression after 24 hours (Fig. 2A). We used bisulfite genomic sequencing, to characterize the methylation status of nine CpG sites located in the U3 region of the HIV LTR, before and after TNF-α treatment. Bisulfite sequencing of the provirus before TNF-α treatment revealed a feature that is typical of CpG methylation (Fig. 2). The 10

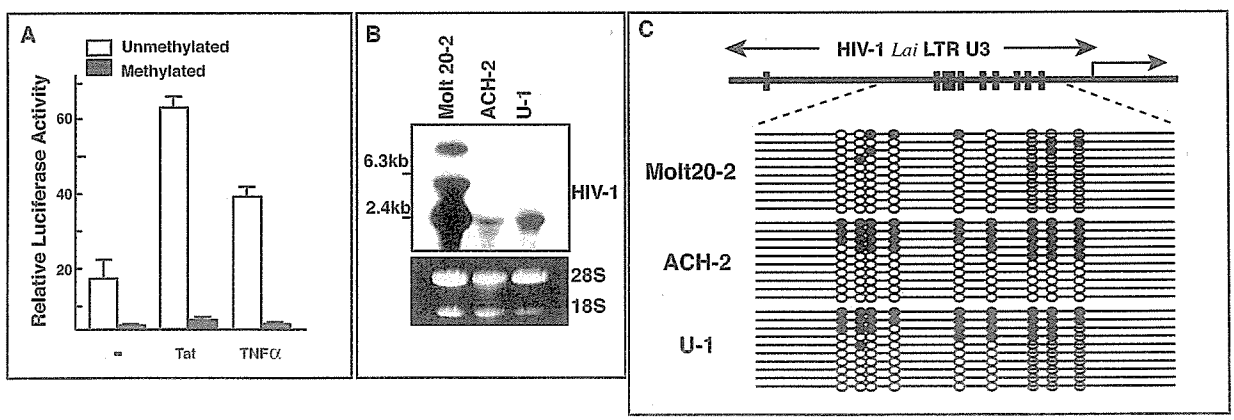


**Figure 1**

Promoter activity and CpG methylation of HIV LTR. **A.** Suppression of HIV LTR promoter activity by CpG methylation *in vitro*. HIV LTR-Luc plasmid, with or without *in vitro* methylation by SssI methylase, was transiently transfected into Jurkat cells with pRL-tk-Luc plasmid. Representative results of triplicate experiments are presented with standard deviation. Relative luciferase activity was determined by dividing the activity of firefly luciferase by that of renilla luciferase. Three independent experiments gave almost identical results. **B.** Northern blot analysis of HIV mRNA. Expression of HIV mRNA was detected using HIV LTR probe (upper panel). Molt20-2 is a gift from Prof. T Shiota (Osaka University) and derived form Molt4 infected by HIV Lai. Lower panel, photograph of ethidium bromide stained samples. **C.** Results of CpG methylation analysis of integrated HIV provirus LTRs of chronically infected cells lines. Single line represents the results of one plasmid clone analyzed. Upper panel, Schematic map of the CpG sites in the U3 region of HIV-1 IIIB LTR. Closed and open circles indicate methylated and unmethylated CpG sites, respectively.

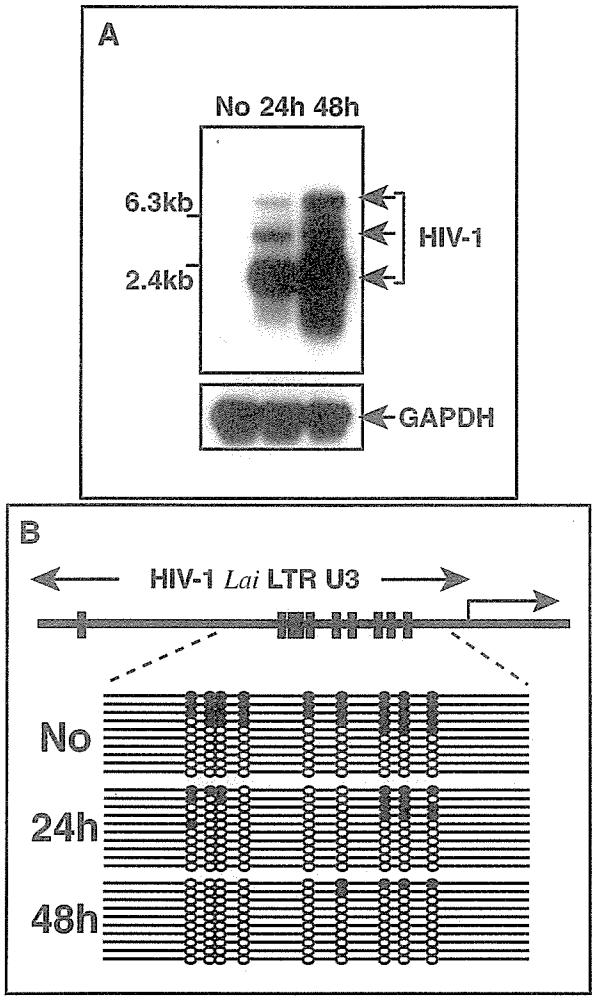


**Figure 2**
*In vitro* induction of HIV gene expression in ACH-2 cells, and demethylation of CpGs in the LTRs. **A**. Induction of HIV mRNA in ACH-2 cell line by TNF-α. Two micrograms of poly (A)+ RNA was analyzed by northern blotting. **B**. CpG demethylation after HIV induction by TNF-α. Upper panel, Schematic map of the CpG sites in the U3 region of HIV-1 IIIB LTR. The lower panel, results of bisulfite genomic sequencing. Cells are harvested at the time points indicated on the left. No, cells without TNF-α treatment. Each line represents a result of single plasmid clone. Closed and open circles indicate methylated and unmethylated CpG sites, respectively.

plasmid clones analyzed displayed either hypermethylation or hypomethylation. Among five hypermethylated clones, three were methylated at all CpGs, and one had 7 out of 9 sites methylated. In DNA extracted from cells after 24 hours of TNF-α treatment, no alleles were completely methylated. Five of 10 sequenced plasmid clones displayed some CpG methylation, and the remaining five clones were completely unmethylated. After 48 hours of TNF-α treatment, there was a clear trend toward demethylation. Eight clones were completely unmethylated, and one had only one methylated CpG (Fig. 2B).

Taken together, the results shown in Fig. 2 can be summarized as follows: 1) at least half of the analyzed clones were unmethylated before and after TNF-α treatment, 2) the levels of CpG methylation in the remaining clones showed a clear decrease that was related to the duration of TNF-α treatment. The primers we used can amplify both 5' and 3' LTR sequences, and methylation of only half of the amplified clones suggests that methylation may affect only the 5' or the 3' LTR, as we found previously in studies of the HTLV-1 provirus [29]. On the other hand, the response to TNF-α provides evidence of cytokine receptor signal-mediated demethylation of the provirus LTR. The mechanism by which LTR is demethylated remains to be elucidated. However, our previous observation in HIV transgenic mice suggested a passive mechanism for demethylation of HIV LTR which depends on DNA replication as is supposed for demethylation of cellular genes[30].

To examine the possibility that hypermethylation is selective for the 5' LTR of the HIV provirus, we first identified the flanking genomic sequences of the integrated provirus in ACH-2 cells using the inverse polymerase chain reaction (I-PCR) [29]. Genomic DNA was digested with a restriction enzyme TthHB8I, followed by self-ligation for 12 hrs. Ligated DNA was subjected to PCR amplification using the following primers: forward primer (iHIV-2): 5'-TTCATCACGTGGCCCGAGAGCTGCATCCGGAGTAC-3' (nucleotide position: 283 to 317), reverse primer (iHIV-1): 5'-CCTTGTGTGTGGTAGATCCACAGATCAAGGATA-3' (nucleotide position: 67 to 37). Agarose gel electrophoresis of the PCR products showed two amplified bands with sizes of about 300 bp and 1,2 kbp. These bands appear to correspond to those from 5'- and 3'-flanking sequences, since ACH-2 cells contain a single copy of integrated HIV provirus per cell [31]. Both PCR products were subcloned using pGEMT-easy (Promega, Madison, Wisconsin) and the nucleotide sequences were determined. The 1.2 kbp PCR product was shown to contain the 5'-LTR sequence, and the 300 bp product that of 3'-LTR. NCBI human genomic blast program analysis of the flanking sequences showed that the sequence of the 1.2 kbp fragment corresponds to that of Chromosome 7, located at 7p15 (Fig.3B). We also identified the 5'-flanking sequences contained the L1 family repetitive sequences (Fig.3B bold italic).

We used the flanking sequences to selectively characterize the CpG methylation status of the 5' LTR, preparing a for-

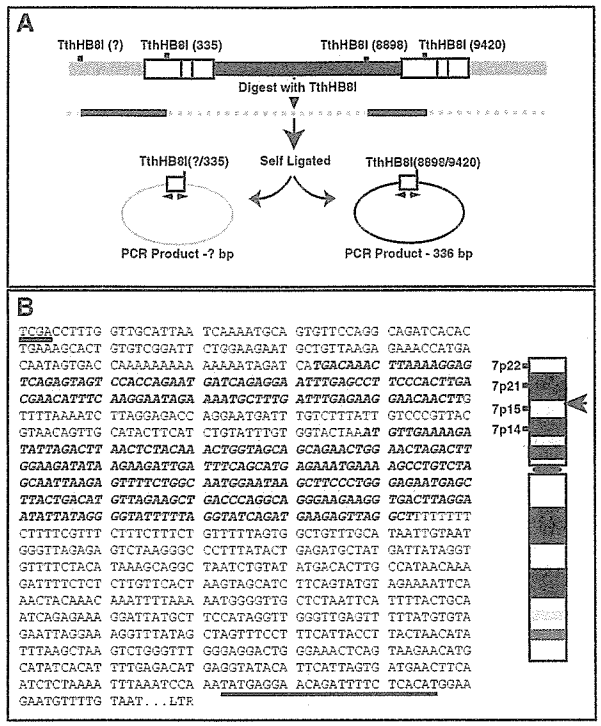


**Figure 3**
Identification of the flanking genomic sequence of the integrated HIV provirus in ACH-2 cells by the inverse PCR. **A**. A schematic chart of the inverse PCR procedure. **B**. Host genomic sequence flanking 5'-LTR. Underlined sequence indicates TthHB8I restriction enzyme site. Double underline indicates the sequence used for the sense primer in 5'-LTR specific methylation analysis. Bold italic indicates the L1 family sequences. Right panel shows a schematic presentation of the chromosomal location of the integration site of HIV-1 in ACH-2 cells determined by the NCBI human genomic blast program. Arrow indicates the region of integration.

ward primer located in the 5' flanking sequence. For analysis of the 3' LTR, we used a forward primer located in the nef region. The primers used are follows: 5' flanking forward primer (5'F-1) 5'-TATGAGGAATAGATTTTTT-TATATG-3' (Fig.3), forward primer for 3' LTR (3'LTR-F1) 5'-TTATAAGGTAGTTGTAGATTTTAGT-3' (nucleotide position 9036 to 9060), and the reverse primer R-1 (described above). The results clearly demonstrated selective hypermethylation of the 5' LTR, with almost complete hypomethylation of the 3' LTR (Fig. 4), which was in accordance with our previous findings with integrated HTLV-1 provirus *in vivo* and *in vitro* [29].

In DNA from unstimulated ACH-2 cells, among 10 clones derived from the 5' LTR, six showed methylation of all 9 CpG sites, and two had only two unmethylated CpGs, although two clones showed complete hypomethylation of the 9 CpG sites. In contrast, all 10 clones derived from the 3' LTR were hypomethylated, with only one methylated site in one clone. The 3' LTR did not show any changes in methylation on TNF-α stimulation (Fig. 4). TNF-α stimulation resulted in increase in unmethylated CpGs in the 5' LTR. After 24 hours of TNF-α stimulation, only one clone out of 10 remained completely methylated, and most clones had one to five unmethylated sites, while one was completely unmethylated. After 48 hours of stimulation, none of the sequenced clones were completely methylated (Fig. 4). Demethylated CpGs appeared to cluster in the first 5 CpG sites (reading 5' to 3'), with higher frequency at the 5th site. Three of 10 clones from unstimulated ACH-2 cells had an unmethylated 5th CpG site, and 6 clones each had unmethylated 5th CpG site after 24 and 48 hours of stimulation. Furthermore, the number of unmethylated CpGs in the first 5 sites increased with the time of TNF-α stimulation. Before stimulation, 12 (24%) of total 50 sites were unmethylated, whereas after stimulation 22 (44%) and 26 (52%) sites were unmethylated at 24 and 48 hours respectively. On the other hand, in the cluster of 4 sites at the 3 end of the cluster, among a total of 40 sites analyzed 8 (20%) were unmethylated in unstimulated cells, and after TNF-α stimulation 6 (15%) and 17 (42.5%) sites were unmethylated at 24 and 48 hours respectively. Taken together, demethylation induced by TNF-α showed a tendency to cluster in the CpG sites located at the 5' end. Furthermore, the 5th CpG site may be a hot spot for demethylation in the TNF-α stimulated cells.

Nevertheless, our results demonstrate that in the setting of full reactivation of viral gene expression by TNF-α stimulation, the provirus LTR showed only a partial demethylation at scattered sites (Fig. 4). This observation is inconsistent with the widely accepted idea that promoter activity is regulated by the density of CpG methylation [22,32,33]. Our results may provide support for the idea that demethylation of a specific CpG site plays an important role in promoter activity of the HIV LTR, which we have previously reported using HIV transgenic mice [30]. It is also consistent with the notion that CpG methylation of specific sites plays an important role in controlling the promoter activities of EBV and imprinted genes [34-38].

Differential methylation of two LTRs located within 10 kbp of each other in the provirus genome, which we previously reported in the human retrovirus HTLV-1 [29], may suggest the presence of an unknown mechanism of methylation targeting that discriminates the 5'from the 3' LTR. The difference may depend on chemical modification of histone H3, such as lysine 9 (K9) methylation, since repression of gene expression mediated by histone

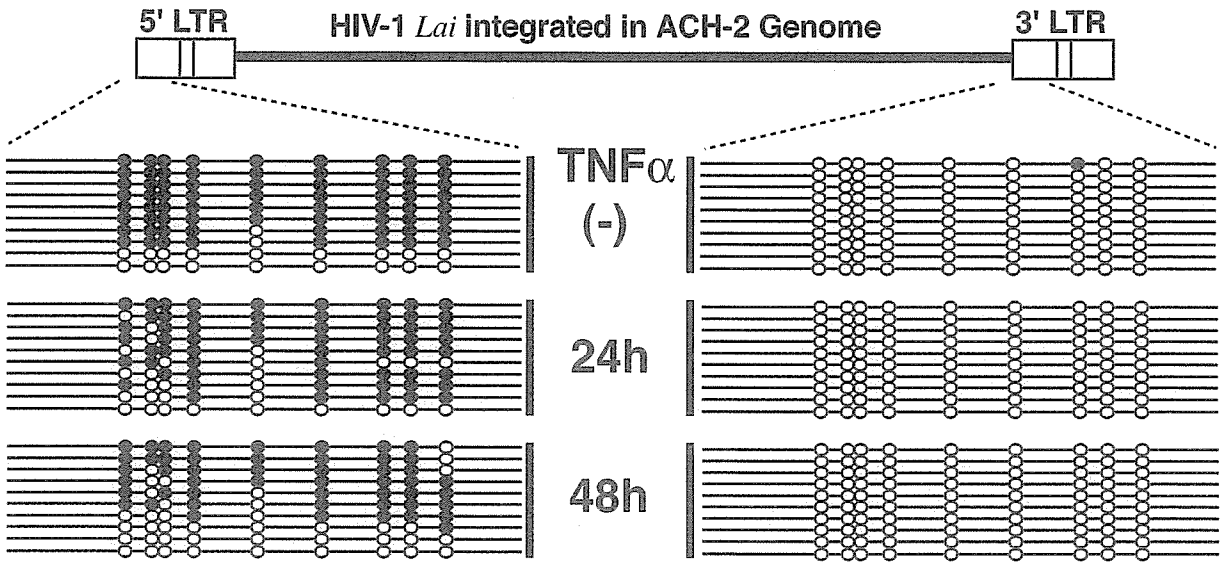


**Figure 4**
Selective analysis of CpG methylation of two LTRs. Methylation of CpG sites in each plasmid clone is displayed. Closed and open circles indicate methylated and unmethylated CpG sites, respectively. TNF-α treated cells are harvested at the time points indicated in the middle. (-), ACH-2 cells harvested before TNF-α treatment.

H3 K9 methylation is thought to be stabilized by DNA methylation[39].

Previous studies *in vitro* suggested CpG methylation of the HIV-1 LTR as a mechanism to maintain HIV-1 latency [20-23,40,41]. However, no information is available as to the CpG methylation status of the HIV provirus in the reservoir pool *in vivo*, because extremely low copy numbers of HIV provirus make it infeasible to directly analyze CpG methylation with bisulfite genomic sequencing. In spite of the widely accepted idea that CpG methylation is involved in suppression of HIV gene expression and latency, a recent report suggested that proviral DNA methylation may not be involved in transcriptional suppression of integrated HIV provirus [42]. However, this report used an artificial system in which provirus methylation was analyzed on a defective HIV genome or a vector having only HIV LTR as the promoter. Because we lack information on the state of the latent HIV provirus *in vivo*, the notion remains to be examined.

Decipherment of the mechanisms for reactivation of latently infected HIV in the reservoir pool will provide the basis for designing treatment strategies for containment or purging of HIV. Thus our observations of 5' LTR selective methylation in ACH-2 cells, and signal-induced demethylation of HIV provirus in the transgenic mice model and latently infected cell lines [30], provide information that will be useful in future investigations.

## Abbreviations
HIV: human immunodeficiency virus

LTR: long terminal repeat

HAART: highly active anti-retrovirus therapy

I-PCR: inverse polymerase chain reaction

## Competing interests
The author(s) declare that they have no competing interests.

## Authors' contributions
T.I. carried out experiments and contributed to data analysis, interpretation, and preparation of figures and drafted the manuscript. A.H. and T.K. carried out part of the experiments including CpG methylation analysis and participated in data analysis and interpretation. T. W. conceived the study, and participated in its design and coordination, and drafted the manuscript.

## Acknowledgements
We thank Drs. David IK Martin and K Suzuki for comments on the manuscript and Ms. S Aizawa and Ms. Maruyama-Nagai for technical assistance. This work was supported by Grants-in-Aid for Scientific Research from the Ministry of Education, Science, Sports and Culture of Japan to T Ishida and T Watanabe, and by a Grant from Japanese Foundation for AIDS Prevention to T Ishida and T Watanabe.

## References


1. Gulick RM, Mellors JW, Havlir D, Eron JJ, Gonzalez C, McMahon D, Richman DD, Valentine FT, Jonas L, Meibohm A, Emini EA, Chodakewitz JA: **Treatment with indinavir, zidovudine, and lamivudine in adults with human immunodeficiency virus infection and prior antiretroviral therapy.** *N Engl J Med* 1997, **337:**734-739.
2. Hammer SM, Squires KE, Hughes MD, Grimes JM, Demeter LM, Currier JS, Eron JJ Jr., Feinberg JE, Balfour HH Jr., Deyton LR, Chodakewitz JA, Fischl MA: **A controlled trial of two nucleoside analogues plus indinavir in persons with human immunodeficiency virus infection and CD4 cell counts of 200 per cubic millimeter or less. AIDS Clinical Trials Group 320 Study Team.** *N Engl J Med* 1997, **337:**725-733.
3. Palella FJ Jr., Delaney KM, Moorman AC, Loveless MO, Fuhrer J, Satten GA, Aschman DJ, Holmberg SD: **Declining morbidity and mortality among patients with advanced human immunodeficiency virus infection. HIV Outpatient Study Investigators.** *N Engl J Med* 1998, **338:**853-860.
4. Detels R, Munoz A, McFarlane G, Kingsley LA, Margolick JB, Giorgi J, Schrager LK, Phair JP: **Effectiveness of potent antiretroviral therapy on time to AIDS and death in men with known HIV infection duration. Multicenter AIDS Cohort Study Investigators.** *Jama* 1998, **280:**1497-1503.
5. Mocroft A, Vella S, Benfield TL, Chiesi A, Miller V, Gargalianos P, d'Arminio Monforte A, Yust I, Bruun JN, Phillips AN, Lundgren JD: **Changing patterns of mortality across Europe in patients infected with HIV-1. EuroSIDA Study Group.** *Lancet* 1998, **352:**1725-1730.
6. Vittinghoff E, Scheer S, O'Malley P, Colfax G, Holmberg SD, Buchbinder SP: **Combination antiretroviral therapy and recent declines in AIDS incidence and mortality.** *J Infect Dis* 1999, **179:**717-720.
7. Perelson AS, Essunger P, Cao Y, Vesanen M, Hurley A, Saksela K, Markowitz M, Ho DD: **Decay characteristics of HIV-1-infected compartments during combination therapy.** *Nature* 1997, **387:**188-191.
8. Chun TW, Stuyver L, Mizell SB, Ehler LA, Mican JA, Baseler M, Lloyd AL, Nowak MA, Fauci AS: **Presence of an inducible HIV-1 latent reservoir during highly active antiretroviral therapy.** *Proc Natl Acad Sci U S A* 1997, **94:**13193-13197.
9. Chun TW, Fauci AS: **Latent reservoirs of HIV: obstacles to the eradication of virus.** *Proc Natl Acad Sci U S A* 1999, **96:**10958-10961.
10. Finzi D, Hermankova M, Pierson T, Carruth LM, Buck C, Chaisson RE, Quinn TC, Chadwick K, Margolick J, Brookmeyer R, Gallant J, Markowitz M, Ho DD, Richman DD, Siliciano RF: **Identification of a reservoir for HIV-1 in patients on highly active antiretroviral therapy.** *Science* 1997, **278:**1295-1300.
11. Wong JK, Hezareh M, Gunthard HF, Havlir DV, Ignacio CC, Spina CA, Richman DD: **Recovery of replication-competent HIV despite prolonged suppression of plasma viremia.** *Science* 1997, **278:**1291-1295.
12. Egger G, Liang G, Aparicio A, Jones PA: **Epigenetics in human disease and prospects for epigenetic therapy.** *Nature* 2004, **429:**457-463.
13. Ylisastigui L, Coull JJ, Rucker VC, Melander C, Bosch RJ, Brodie SJ, Corey L, Sodora DL, Dervan PB, Margolis DM: **Polyamides reveal a role for repression in latency within resting T cells of HIV-infected donors.** *J Infect Dis* 2004, **190:**1429-1437.
14. Lehrman G, Hogue IB, Palmer S, Jennings C, Spina CA, Wiegand A, Landay AL, Coombs RW, Richman DD, Mellors JW, Coffin JM, Bosch RJ, Margolis DM: **Depletion of latent HIV-1 infection in vivo: a proof-of-concept study.** *Lancet* 2005, **366:**549-555.
15. Smith SM: **Valproic acid and HIV-1 latency: beyond the sound bite.** *Retrovirology* 2005, **2:**56.
16. Harbers K, Schnieke A, Stuhlmann H, Jahner D, Jaenisch R: **DNA methylation and gene expression: endogenous retroviral genome becomes infectious after molecular cloning.** *Proc Natl Acad Sci U S A* 1981, **78:**7609-7613.
17. Hu WS, Fanning TG, Cardiff RD: **Mouse mammary tumor virus: specific methylation patterns of proviral DNA in normal mouse tissues.** *J Virol* 1984, **49:**66-71.
18. Li E, Beard C, Jaenisch R: **Role for DNA methylation in genomic imprinting.** *Nature* 1993, **366:**362-365.
19. Niwa O, Sugahara T: **5-Azacytidine induction of mouse endogenous type C virus and suppression of DNA methylation.** *Proc Natl Acad Sci U S A* 1981, **78:**6290-6294.
20. Bednarik DP, Mosca JD, Raj NB: **Methylation as a modulator of expression of human immunodeficiency virus.** *J Virol* 1987, **61:**1253-1257.
21. Bednarik DP, Cook JA, Pitha PM: **Inactivation of the HIV LTR by DNA CpG methylation: evidence for a role in latency.** *Embo J* 1990, **9:**1157-1164.
22. Gutekunst KA, Kashanchi F, Brady JN, Bednarik DP: **Transcription of the HIV-1 LTR is regulated by the density of DNA CpG methylation.** *J Acquir Immune Defic Syndr* 1993, **6:**541-549.
23. Schulze-Forster K, Gotz F, Wagner H, Kroger H, Simon D: **Transcription of HIV1 is inhibited by DNA methylation.** *Biochem Biophys Res Commun* 1990, **168:**141-147.
24. Folks TM, Justement J, Kinter A, Dinarello CA, Fauci AS: **Cytokine-induced expression of HIV-1 in a chronically infected promonocyte cell line.** *Science* 1987, **238:**800-802.
25. Folks TM, Clouse KA, Justement J, Rabson A, Duh E, Kehrl JH, Fauci AS: **Tumor necrosis factor alpha induces expression of human immunodeficiency virus in a chronically infected T-cell clone.** *Proc Natl Acad Sci U S A* 1989, **86:**2365-2368.
26. Chun TW, Engel D, Mizell SB, Ehler LA, Fauci AS: **Induction of HIV-1 replication in latently infected CD4+ T cells using a combination of cytokines.** *J Exp Med* 1998, **188:**83-91.
27. Chun TW, Engel D, Mizell SB, Hallahan CW, Fischette M, Park S, Davey RT Jr., Dybul M, Kovacs JA, Metcalf JA, Mican JM, Berrey MM, Corey L, Lane HC, Fauci AS: **Effect of interleukin-2 on the pool of latently infected, resting CD4+ T cells in HIV-1-infected patients receiving highly active anti-retroviral therapy.** *Nat Med* 1999, **5:**651-655.
28. Clark SJ, Harrison J, Paul CL, Frommer M: **High sensitivity mapping of methylated cytosines.** *Nucleic Acids Res* 1994, **22:**2990-2997.
29. Koiwa T, Hamano-Usami A, Ishida T, Okayama A, Yamaguchi K, Kamihira S, Watanabe T: **5'-long terminal repeat-selective CpG methylation of latent human T-cell leukemia virus type I provirus in vitro and in vivo.** *J Virol* 2002, **76:**9389-9397.
30. Tanaka J, Ishida T, Choi BI, Yasuda J, Watanabe T, Iwakura Y: **Latent HIV-1 reactivation in transgenic mice requires cell cycle - dependent demethylation of CREB/ATF sites in the LTR.** *Aids* 2003, **17:**167-175.
31. Poli G, Kinter A, Justement JS, Kehrl JH, Bressler P, Stanley S, Fauci AS: **Tumor necrosis factor alpha functions in an autocrine manner in the induction of human immunodeficiency virus expression.** *Proc Natl Acad Sci U S A* 1990, **87:**782-785.
32. Boyes J, Bird A: **Repression of genes by DNA methylation depends on CpG density and promoter strength: evidence for involvement of a methyl-CpG binding protein.** *Embo J* 1992, **11:**327-333.
33. Hsieh CL: **Dependence of transcriptional repression on CpG methylation density.** *Mol Cell Biol* 1994, **14:**5487-5494.
34. Iannello RC, Young J, Sumarsono S, Tymms MJ, Dahl HH, Gould J, Hedger M, Kola I: **Regulation of Pdha-2 expression is mediated by proximal promoter sequences and CpG methylation.** *Mol Cell Biol* 1997, **17:**612-619.
35. Jansson A, Masucci M, Rymo L: **Methylation of discrete sites within the enhancer region regulates the activity of the Epstein-Barr virus BamHI W promoter in Burkitt lymphoma lines.** *J Virol* 1992, **66:**62-69.
36. Mancini DN, Rodenhiser DI, Ainsworth PJ, O'Malley FP, Singh SM, Xing W, Archer TK: **CpG methylation within the 5' regulatory region of the BRCA1 gene is tumor specific and includes a putative CREB binding site.** *Oncogene* 1998, **16:**1161-1169.
37. Mancini DN, Singh SM, Archer TK, Rodenhiser DI: **Site-specific DNA methylation in the neurofibromatosis (NF1) promoter interferes with binding of CREB and SP1 transcription factors.** *Oncogene* 1999, **18:**4108-4119.
38. Robertson KD, Hayward SD, Ling PD, Samid D, Ambinder RF: **Transcriptional activation of the Epstein-Barr virus latency C promoter after 5-azacytidine treatment: evidence that demethylation at a single CpG site is crucial.** *Mol Cell Biol* 1995, **15:**6150-6159.
39. Richards EJ, Elgin SC: **Epigenetic codes for heterochromatin formation and silencing: rounding up the usual suspects.** *Cell* 2002, **108:**489-500.

40. O'Brien MC, Ueno T, Jahan N, Zajac-Kaye M, Mitsuya H: **HIV-1 expression induced by anti-cancer agents in latently HIV-1-infected ACH2 cells.** *Biochem Biophys Res Commun* 1995, **207:**903-909.
41. Singh MK, Pauza CD: **Extrachromosomal human immunodeficiency virus type 1 sequences are methylated in latently infected U937 cells.** *Virology* 1992, **188:**451-458.
42. Pion M, Jordan A, Biancotto A, Dequiedt F, Gondois-Rey F, Rondeau S, Vigne R, Hejnar J, Verdin E, Hirsch I: **Transcriptional suppression of in vitro-integrated human immunodeficiency virus type 1 does not correlate with proviral DNA methylation.** *J Virol* 2003, **77:**4025-4032.

Publish with BioMed Central and every scientist can read your work free of charge

*"BioMed Central will be the most significant development for disseminating the results of biomedical research in our lifetime."*

Sir Paul Nurse, Cancer Research UK

Your research papers will be:

- available free of charge to the entire biomedical community
- peer reviewed and published immediately upon acceptance
- cited in PubMed and archived on PubMed Central
- yours — you keep the copyright

Submit your manuscript here:
http://www.biomedcentral.com/info/publishing_adv.asp

BioMedcentral

## Intraocular soluble IL-2 receptor alpha in a patient with adult T cell leukaemia with intraocular invasion

It has been reported that human T cell lymphotropic virus type I (HTLV-I) infection is related to a wide range of ocular disorders, such as intraocular lymphoma,[1 2] uveitis,[3] and cytomegalovirus (CNV) retinitis.[4] The diagnosis of adult T cell leukaemia (ATL) cell infiltration in the eye is often difficult, even when characteristic ocular findings are present and cytological examinations of intraocular fluids are performed. It is well known that determination of patient serum interleukin 2 receptor alpha (sIL-2Rα) levels is critical in the evaluation of the clinical status of the disease.[5] We report here a patient with systemic ATL who developed vitreous opacities and subretinal lesions and in whom vitreous measurement of the soluble form of sIL-2Rα provided information that could be used in making a diagnosis and in treating associated ocular disorders.

### Case report

A 69 year old man with a 2 year history of systemic ATL developed a sudden onset of decreased vision and vitreous floaters in the left eye. Funduscopic examination of the left eye revealed dense vitreous opacities and whitish retinal exudates along with superior vascular arcade (fig 1A). Based on the ocular manifestations and the presence of systemic ATL, intraocular infiltration of ATL cells was suspected and a diagnostic pars plana vitrectomy was performed in the left eye. After informed consent was obtained, a vitreous sample from the patient was analysed using research protocol. The cytopathology of the vitreous sample was class III with many atypical lymphoid cells. The extra cell pellet of the sample was used for polymerase chain reaction (PCR). Proviral DNA for the HTLV-I tax gene was amplified using previously described PCR methods.[3] The proviral DNA was amplified by PCR (fig 1B). We also examined detection of CMV-DNA using quantitative PCR, because diffuse dot retinal haemorrhages like a CMV retinitis were seen in the left eye. The result of quantitative PCR was undetectable levels in the vitreous. Since the HTLV-I tax gene was detected in the vitreous sample, the vitreous fluid was assayed for sIL-2Rα levels using ELISA (R&D system, Minneapolis, MN, USA). Data for the vitreous samples of seven patients with various retinal disorders, who served as controls, can be seen in figure 2. In this patient, the concentrations of sIL-2Rα were extremely high (115 114 pg/ml) in the vitreous and considerably high in the serum. The concentrations of sIL-2Rα in the vitreous and the serum of another ATL patient with CMV retinitis, in a patient with intraocular B cell lymphoma, and in a patient with sarcoidosis or HTLV-I associated uveitis (HTLV-I carrier, no ATL) were also high, although the concentrations were much less than that observed in the vitreous of this case (fig 2). In addition, detectable levels of sIL-2Rα were not observed in patients with toxocariasis, idiopathic macular hole or non-PVR retinal detachment.

Our ATL patient had received conventional CHOP therapy before observation of the ocular symptoms. After identification of the ocular ATL infiltrates and documentation of sIL-2Rα, a cerebrospinal injection of anticancer medication containing a combination of methotrexate, cytarabine, and prednisolone was added to the CHOP therapy because the patient had central nervous system involvement. One month later, a dramatic improvement was noted in the patient with regard to the retinal exudates and haemorrhages (fig 1C).

### Comment

In the current case, the sIL-2Rα level was much higher than the level observed in the serum or in the vitreous of patients with other retinal disorders. These data strongly suggest that the infiltrating T cell leukaemic cells constitutively express IL-2Rα on their surface, and secrete soluble forms of IL-2Rα into the vitreous. Also, the results of this case suggest that the measurement of sIL-2Rα in the vitreous could be a useful tool in the diagnosis of direct invasion of ATL in the eye, which is critical in the prognosis for the eye and for death.

HTLV-I infection is endemic in Japan, the Caribbean islands, and South America. Known ophthalmic manifestations of HTLV-I include malignant infiltrates in patients with ATL, neuro-ophthalmic disorders, and HTLV-I associated uveitis. Most of the published information on HTLV-I ocular manifestations comes from cases in south western Japan, which currently has the highest incidence of infection worldwide. Routine evaluation of HTLV-I infected patients is important because immune mediated or neoplastic ocular involvement may occur during the course of the disease. In different populations, genetic and environmental factors may also have a role in the ocular manifestations of HTLV-I.

Unlike ocular ATL infiltrates, HTLV-I associated uveitis is not a serious disorder, as this condition is responsive to corticosteroid therapy. However, since patients with ATL infected by HTLV-I are immunocompromised and subject to invasion of retinal lesions[1 2] and cytomegalovirus retinitis,[4] early diagnosis and treatment are very important. In the present ATL case, the early diagnosis helped to ensure that the patient was able to receive an appropriate course of therapy.

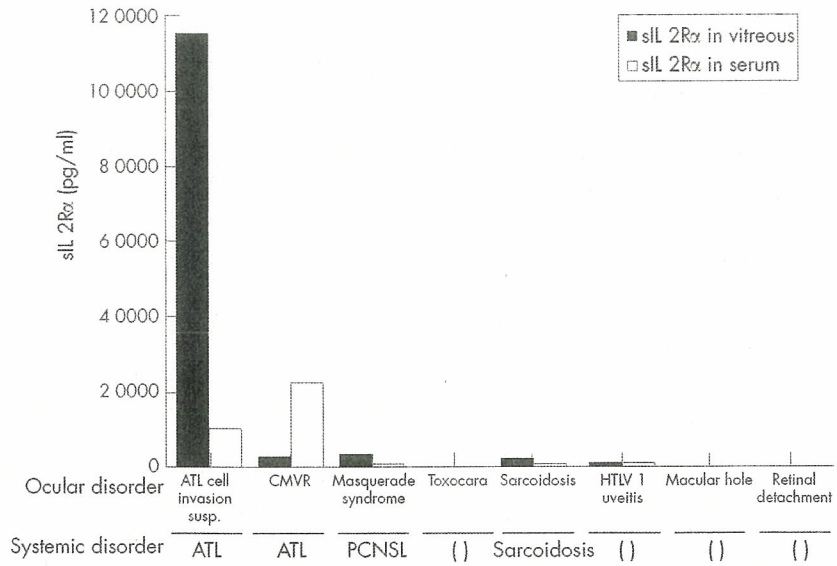


**Figure 2** Soluble IL-2 receptor alpha (sIL-2Rα) concentrations in the vitreous and the serum of patients with various ocular diseases. CMVR, cytomegarovirus retinitis; ATL, adult T cell leukaemia/lymphoma; PCNSL, primary central nervous system lymphoma (malignant B cell lymphoma); Toxocara, toxocariasis; HTLV-I uveitis, HTLV-I associated uveitis; Macular hole, idiopathic macular hole.

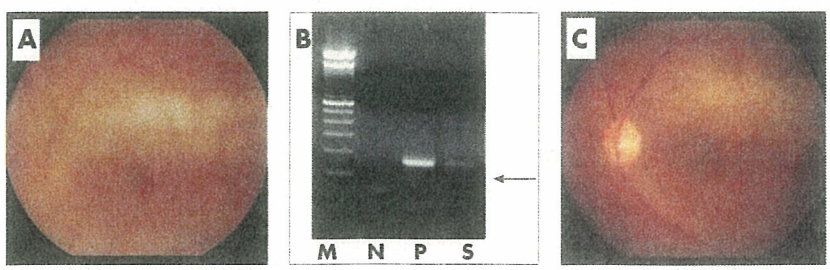


**Figure 1** Fundus photographs and PCR results. (A) Fundus photograph showing retinal whitish lesions along retinal vessels and dense vitreous opacities. (B) Detection of proviral DNA of HTLV-I tax gene in vitreous of our ATL patient. M, molecular size marker, N, negative control, P, positive control (HTLV-I infected cells), S, vitreous sample of our ATL patient. (C) Fundus photograph after treatment with chemotherapy of anticancer medication and CHOP therapy. The cells are not present.

## Acknowledgements

We thank Dr Duco Hamasaki for critical reading of this manuscript. Partial financial support was from Scientific Research (B) 1437055 of the Ministry of Education, Culture, Sports, Science and Technology, Japan.

**S Sugita, H Takase, T Yoshida, Y Sugamoto**
Department of Ophthalmology and Visual Science, Tokyo Medical and Dental University Graduate School of Medicine, Tokyo, Japan

**T Watanabe**
Laboratory of Tumor Cell Biology, Department of Medical Genome Sciences, Graduate School of Frontier Sciences, University of Tokyo, Tokyo, Japan

**M Mochizuki**
Department of Ophthalmology and Visual Science, Tokyo Medical and Dental University Graduate School of Medicine, Tokyo, Japan

Correspondence to: Dr S Sugita, Department of Ophthalmology and Visual Science, Tokyo Medical and Dental University Graduate School of Medicine, 1-5-45 Yushima, Bunkyo-ku, Tokyo 113-8519, Japan; sunaoph@tmd.ac.jp

doi: 10.1136/bjo.2006.092809

Accepted for publication 18 March 2006

## References

1 **Hirata A**, Miyazaki T, Tanihara H. Intraocular infiltration of adult T-cell leukemia. *Am J Ophthalmol* 2002;**134**:616–28.
2 **Kumar SR**, Gill PS, Wagner DG, *et al*. Human T-cell lymphotropic virus type I-associated retinal lymphoma. A clinicopathologic report. *Arch Ophthalmol* 1994;**112**:954–9.
3 **Sagawa K**, Mochizuki M, Masuoka K, *et al*. Immunopathological mechanisms of human T cell lymphotropic virus type 1 (HTLV-I) uveitis; detection of HTLV-I- infected T cells in the eye and their constitutive cytokine production. *J Clin Invest* 1995;**95**:852–8.
4 **Mori N**, Ura K, Murakami S, *et al*. Adult T cell leukemia with cytomegalovirus retinitis. *Rinsho Ketsueki* 1992;**33**:537–41.
5 **Yamaguchi K**, Nishimura Y, Kiyokawa T, *et al*. Elevated serum levels of soluble interleukin-2 receptors in HTLV-I-associated myelopathy. *J Lab Clin Med* 1989;**114**:407–11.

*Journal of General Virology* (2006), 87, 1311–1320 DOI 10.1099/vir.0.81307-0

# Rapid dissemination of a pathogenic simian/human immunodeficiency virus to systemic organs and active replication in lymphoid tissues following intrarectal infection

Ariko Miyake,[1,2] Kentaro Ibuki,[1] Yoshimi Enose,[1] Hajime Suzuki,[1] Reii Horiuchi,[1] Makiko Motohara,[1] Naoki Saito,[1] Tadashi Nakasone,[3] Mitsuo Honda,[3] Toshiki Watanabe,[2] Tomoyuki Miura[1] and Masanori Hayami[1]

Correspondence
Masanori Hayami
mhayami@virus.kyoto-u.ac.jp

[1]Institute for Virus Research, Laboratory of Primate Model, Experimental Research Center for Infectious Disease, Kyoto University, Sakyo-ku, Kyoto 606-8507, Japan

[2]Laboratory of Tumor Cell Biology, Department of Medical Genome Sciences, Graduate School of Frontier Sciences, The University of Tokyo, Tokyo 108-8639, Japan

[3]National Institute of Infectious Disease, Tokyo 162-8640, Japan

A better understanding of virological events during the early phase of human immunodeficiency virus 1 (HIV-1) infection is important for development of effective antiviral vaccines. In this study, by using quantitative PCR and an infectious plaque assay, virus distribution and replication were examined in various internal organs of rhesus macaques for almost 1 month after intrarectal inoculation of a pathogenic simian immunodeficiency virus/HIV chimeric virus (SHIV-C2/1-KS661c). At 3 days post-inoculation (p.i.), proviral DNA was detected in the rectum, thymus and axillary lymph node. In lymphoid tissues, infectious virus was first detected at 6 days p.i. and a high level of proviral DNA and infectious virus were both detected at 13 days p.i. By 27 days p.i., levels of infectious virus decreased dramatically, although proviral DNA load remained unaltered. In the intestinal tract, levels of infectious virus detected were much lower than in lymphoid tissues, whereas proviral DNA was detected at the same level as in lymphoid tissues throughout the infection. In the thymus and jejunum, CD4CD8 double-positive T cells were depleted earlier than CD4 single-positive cells. These results show that the virus spread quickly to systemic tissues after mucosal transmission. Thereafter, infectious virus was actively produced in the lymphoid tissues, but levels decreased significantly after the peak of viraemia. In contrast, in the intestinal tract, infectious virus was produced at low levels from the beginning of infection. Moreover, virus pathogenesis differed in CD4 single-positive and CD4CD8 double-positive T cells.

Received 1 July 2005
Accepted 9 January 2006

## INTRODUCTION

A better understanding of virological events during the early phase of human immunodeficiency virus 1 (HIV-1) infection is essential for the development of effective vaccines for preventing virus transmission. This is especially true for mucosal infections, which are the major mode of HIV-1 transmission. Moreover, high virus load in the early phase of infection has been reported to correlate with earlier onset of AIDS (Fauci, 1996; Mellors *et al.*, 1995; Schacker *et al.*, 1996). Therefore, data obtained from the early phase of infection would help to define the pathogenesis of HIV-1.

Several non-human primate models have been used to investigate the early phase of HIV-1 infection (Joag *et al.*, 1997; Lu *et al.*, 1998). In some studies using macaques inoculated with *Simian immunodeficiency virus* (SIV) or an SIV/HIV-1 chimeric virus (SHIV) by a mucosal route (i.e. oral, rectal or vaginal), the virus spread to the systemic lymphoid tissues within 3–7 days post-inoculation (p.i.) following replication for a period of time in the local region (Couëdel-Courteille *et al.*, 1999, 2003; Hirsch *et al.*, 1998; Spira *et al.*, 1996; Stahl-Hennig *et al.*, 1999). However, recent studies have shown that the virus can spread more rapidly to the systemic tissues. Hu *et al.* (2000) detected SIV-infected cells in draining lymph nodes within 18 h of intravaginal exposure. Milush *et al.* (2004) showed that SIV spread to systemic lymphoid tissues 1–2 days after oral inoculation. Miller *et al.* (2005) showed that the dissemination of SIV infection to systemic lymphoid tissues occurred within 1–3 days of vaginal inoculation, although virus production

at this site was established later. Furthermore, Veazey *et al.* (1998) reported that the intestinal tract was one of the major sites of SIV replication and $CD4^+$ T cell depletion in the early phase of infection. In a study using SHIV, Harouse *et al.* (1999) suggested that SHIV using CCR5 as co-receptor for virus entry caused a dramatic loss of $CD4^+$ intestinal T cells followed by a gradual depletion in peripheral $CD4^+$ T cells, whereas infection with SHIV using CXCR4 caused a profound loss in peripheral T cells that was not paralleled in the intestine.

The goals of the present study were to investigate the distribution of pathogenic virus in systemic tissues early after mucosal infection and to determine whether these tissues produced infectious virus, which is considered to play a major role in the spread of virus in the body. A pathogenic molecular clone, SHIV-C2/1-KS661c (Shinohara *et al.*, 1999), which uses two major chemokine receptors, CCR5 and CXCR4, as co-receptors for virus entry, was used to inoculate rhesus macaque monkeys intrarectally. Proviral DNA and infectious virus were quantified by quantitative PCR and infectious plaque assay, respectively. Virus load in the infected individuals has usually been quantified by the copy number of virus RNA or DNA using PCR or by the immunodetection of core protein, p24 or p27 (Chun *et al.*, 1997; Sei *et al.*, 1994; Zhang *et al.*, 1999). However, these methods do not differentiate between infectious and non-infectious virus. The infectious plaque assay used in this study quantified infectious virus only (Kato *et al.*, 1998; Miyake *et al.*, 2004). Our results show that the virus spread rapidly to the systemic tissues soon after intrarectal infection. Thereafter, infectious virus was actively produced in the lymphoid tissues, but decreased significantly after the peak of viraemia. In the intestinal tract, lower levels of infectious virus were produced than in lymphoid tissues throughout the infection.

## METHODS

**Virus.** SHIV-C2/1 was generated by *in vivo* passage of SHIV-89.6 (containing *env*, *tat*, *rev* and *vpu* derived from primary isolates of HIV-1) (Shinohara *et al.*, 1999). SHIV-C2/1-KS661c is a molecular clone constructed from the consensus sequence of SHIV-C2/1 (GenBank accession no. AF217181). SHIV-C2/1-KS661c can infect macaque monkeys by intravenous and intrarectal routes and cause precipitous viraemia and drastic $CD4^+$ cell depletion. Virus stock was prepared from supernatant of a human lymphoid cell line, CEMx174, and stored in liquid nitrogen (−190 °C) until use. The $TCID_{50}$ of the virus stock was measured in CEMx174; 20 $TCID_{50}$ was equivalent to one 50 % macaque infectious dose ($MID_{50}$).

**Monkeys and virus inoculation.** Ten adult (5- to 8-year-old) rhesus macaques (*Macaca mulatta*), which were of Chinese origin, were used in this study. All monkeys used were treated in accordance with the institutional regulations approved by the Committee for Experimental Use of Non-human Primates in the Institute for Virus Research, Kyoto University. Eight monkeys were anaesthetized by intramuscular injection of ketamine chloride and inoculated intrarectally with $2 \times 10^3$ $TCID_{50}$ SHIV-C2/1-KS661c. All intrarectal inoculations were done with a paediatric feeding catheter 10 cm from the anus. The catheter was inserted carefully to avoid causing trauma. Two monkeys were euthanized at each of 3 (animals MM301 and MM307), 6 (MM300 and MM309), 13 (MM313 and MM334) and 27 (MM308 and MM310) days p.i. Two monkeys (MM244 and MM314) were used as uninfected controls.

**Sample collection.** Blood was collected periodically from all monkeys. Peripheral blood mononuclear cells (PBMCs) and plasma were separated from heparinized blood by Percoll (Lymphocyte Separation Solution; Nacalai Tesque) density-gradient centrifugation. Plasma was frozen at −80 °C until use. Complete sets of organs were obtained at the time of euthanasia. Parts of the samples were frozen directly at −80 °C until further use (i.e. quantification of proviral DNA). Residual samples of spleen, thymus, and axillary, inguinal and mesenteric lymph nodes were minced and filtered through a 40 μm nylon filter (Becton Dickinson). Samples of jejunum and rectum were washed in Dulbecco's modified Eagle's medium (DMEM) containing 0·45 mM dithiothreitol, cut into 1 $cm^2$ pieces and agitated in DMEM medium containing 5 % fetal calf serum (FCS) for 1 h at room temperature. After short sedimentation, supernatants and tissue fragments were processed to give intraepithelial lymphocytes (iEL) and lamina propria lymphocytes (LPL), respectively. The supernatants (containing iEL) were filtered through columns containing packed glass wool and centrifuged at 1600 r.p.m. for 7 min; pellets were then suspended in 30 % Percoll (Pharmacia) and centrifuged at 1800 r.p.m. for 20 min. The resulting pellets were resuspended in 44 % Percoll, layered on 70 % Percoll and centrifuged at 1800 r.p.m. for 20 min. Cells at the interface between the 44 and 70 % Percoll layers were collected. The residual tissue fragments were agitated in Hanks' buffer containing 5 mM EDTA for 10 min at room temperature and the supernatants were removed. This step was repeated three times. The fragments were suspended in RPMI 1640 medium (Gibco) containing 10 % FCS and, after agitation for 30 min at room temperature, the supernatants were removed. The fragments were resuspended in RPMI 1640 medium containing 10 % FCS and type II collagenase (0·2 mg $ml^{-1}$; Sigma) and agitated for 90 min at room temperature. The suspensions (containing LPL) were filtered through glass-wool columns and cells were enriched by Percoll density-gradient centrifugation as described above for iEL. The cells obtained from each organ were used immediately in the infectious plaque assay and flow-cytometry analysis.

**Quantification of plasma viral RNA.** The viral RNA loads in plasma were determined by quantitative RT-PCR (Suryanarayana *et al.*, 1998). Total RNAs were prepared from plasma with a QIAamp Viral RNA kit (QIAGEN). RT-PCR was performed with a Taqman EZ RT-PCR kit (Perkin Elmer) for the SIV *gag* region using the following primers: SIV2-696F (5′-GGAAATTACCCAGTACAACAAATAGG-3′) and SIV2-784R (5′-TCTATCAATTTTACCCAGGCATTTA-3′). A labelled probe, SIV2-731T (5′-Fam-TGTCCACCTGCCATTAAGCCCG-Tamra-3′; Perkin Elmer), was used for detection of the PCR products. These reactions were performed with a Prism 7700 Sequence Detector (Applied Biosystems) and analysed by using the manufacturer's software. For each run, a standard curve was generated from dilutions whose copy numbers were known and the RNA in the plasma samples was quantified based on the standard curve.

**Quantification of proviral DNA.** Proviral DNA loads in tissues were determined by quantitative PCR. DNA samples were extracted directly from frozen tissues with a Qiagen DNeasy Tissue kit. PCR was performed with a Taqman PCR Reagent kit (Perkin Elmer) using the same primer set and probe used in RT-PCR. A standard curve was generated from a plasmid DNA sample containing the full genome of SHIV-NM-3rN, which was quantified with a UV spectrophotometer.

**Infectious plaque assay.** Infectious virus was quantified and isolated by using an infectious plaque assay (Kato *et al.*, 1998). An

agarose-gel bilayer containing RPMI 1640 medium was made in plastic culture dishes with a diameter of 100 mm; the lower layer consisted of 12 ml 1·2% agarose (Agarose NA; Pharmacia) and the upper layer consisted of 12 ml 0·4% low gelling-temperature agarose (SeaPlaque Agarose; FMC). Dishes were incubated at 37 °C in 5% $CO_2$ overnight. The following day, $2 \times 10^6$ cells of each sample and $8 \times 10^6$ M8166 cells (Clapham *et al.*, 1987) were suspended in 3 ml 0·4% low gelling-temperature agarose solution containing the culture medium and the mixture was immediately overlaid on the agarose-gel layer prepared previously. After the gel had hardened, plates were covered with 12 ml culture medium and incubated at 37 °C in 5% $CO_2$ for 10 days. The medium over the plates was replaced with fresh medium every day. After removal of the medium on day 10, plates were stained with 2 ml 0·7% MTT for 2 h to count the number of plaques.

**Flow-cytometry analysis.** The frequencies of $CD4^+$ single-positive and CD4CD8 double-positive T cells in PBMCs and various tissues were examined by flow cytometry. Lymphocytes were treated with anti-CD3 (FN-18–fluorescein isothiocyanate; Biosource), anti-CD4 (Nu-TH/I–phycoerythrin; NICHIREI) and anti-CD8 (SK1–PerCP; Becton-Dickinson) monoclonal antibodies and examined on a FACScan analyser (Becton Dickinson). The absolute number of lymphocytes in the blood was determined by using an automated blood-cell counter (F-820; Sysmex).

## RESULTS

### Intrarectal infection of macaque monkeys with SHIV-C2/1-KS661c

Eight rhesus macaque monkeys were inoculated intrarectally with SHIV-C2/1-KS661c and two monkeys were euthanized at each of 3, 6, 13 and 27 days p.i. In the two monkeys that were euthanized at 3 days p.i. (MM301 and MM307), plasma viral RNA was not detected in the time between inoculation and euthanasia. However, plasma viral RNA was first detected at 3 days p.i. in one monkey (MM300) and at 6 or 7 days p.i. in five monkeys (MM309, MM313, MM334, MM308 and MM310) (Fig. 1). The plasma viral RNA load of these monkeys reached peak levels, about $10^8$ to $5 \times 10^9$ copies $ml^{-1}$, at 13 days p.i. and then decreased, reaching $10^6$ copies $ml^{-1}$ at 27 days p.i. $CD4^+$ T-cell counts in peripheral blood of these monkeys started to decrease from day 6 p.i. and were lower than 500 cells $\mu l^{-1}$ by 13 days p.i. (Fig. 2). These low counts of $CD4^+$ T cells remained at the same levels until 27 days p.i.

### Detection of proviral DNA in various tissues early after intrarectal inoculation

To investigate virus distribution to the systemic tissues early after infection, proviral DNAs in various tissues were determined by quantitative PCR. Proviral DNA was already detected at 3 days p.i. in the rectum and distal lymphoid tissues (thymus and axillary lymph node) of one monkey examined at this time (MM301) (Fig. 3). It was also detected in non-lymphoid tissues (kidney and lung; data not shown) at low levels [$<20$ copies $(\mu g\ DNA)^{-1}$]. These results show that the virus spread quickly to the systemic tissues after intrarectal inoculation. In both monkeys that were examined at 6 days p.i. (MM300 and MM309), proviral

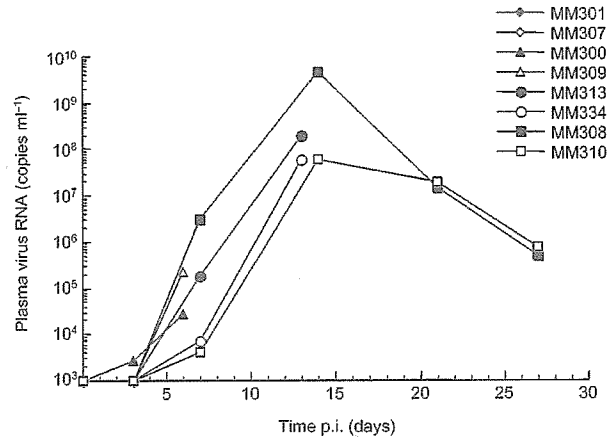


**Fig. 1.** Plasma viral RNA loads of eight monkeys inoculated intrarectally with SHIV-C2/1-KS661c. MM301 and MM307, MM300 and MM309, MM313 and MM334, and MM308 and MM310 were euthanized at 3, 6, 13 and 27 days p.i., respectively. The detection limit of this assay was $1 \times 10^3$ copies $ml^{-1}$.

DNA was detected in PBMCs as well as other lymphoid tissues (Fig. 3), suggesting that detectable levels of infected cells had drained to the peripheral bloodstream by this time. However, the titres of proviral DNA in these tissues were less than about $10^2$ copies $(\mu g\ DNA)^{-1}$ and proviral DNA was not detected in some tissues at 6 days p.i. In monkeys examined at 13 days p.i. (MM313 and MM334), when viraemia reached peak levels, proviral DNA was detected in all tissues examined and virus titres in each tissue were much higher than those determined at 6 days p.i. In most of the lymphoid tissues and the intestinal tract, proviral DNA was detected at $>10^3$ copies $\mu g^{-1}$ (Fig. 3). In the non-lymphoid tissues of these monkeys, including lung, liver, kidney and

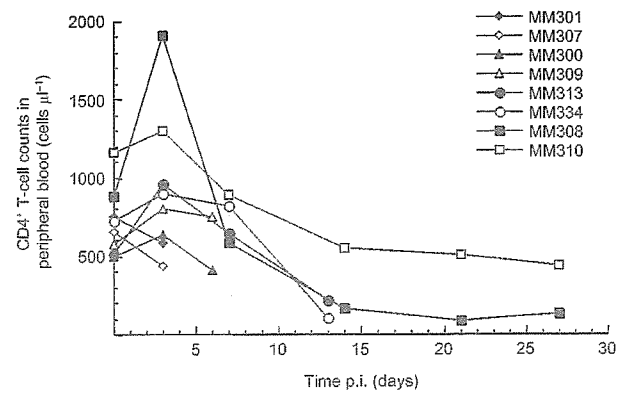


**Fig. 2.** Number of $CD4^+$ T cells in peripheral blood of eight monkeys inoculated intrarectally with SHIV-C2/1-KS661c. MM301 and MM307, MM300 and MM309, MM313 and MM334, and MM308 and MM310 were euthanized at 3, 6, 13 and 27 days after inoculation, respectively.

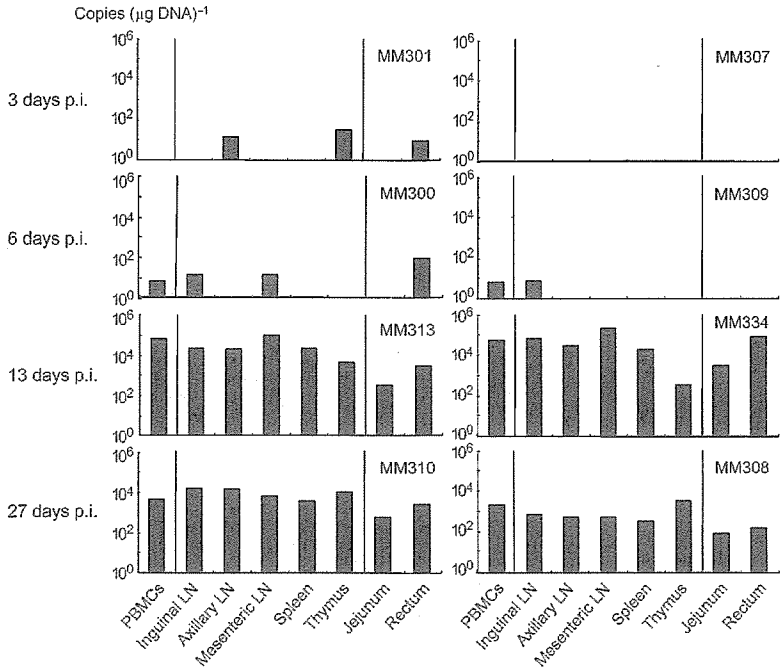


**Fig. 3.** Proviral DNA loads in various tissues of eight SHIV-C2/1-KS661c-inoculated monkeys. Virus loads were determined by quantitative PCR and are expressed as viral DNA copy numbers (μg total DNA extracted from tissue homogenates)$^{-1}$.

brain, proviral DNA was detected at about 10–$10^3$ copies $\mu g^{-1}$ (data not shown). The titres of proviral DNA in all tissues of the monkeys examined at 27 days p.i. (MM308 and MM310) were still $>10^3$ copies $\mu g^{-1}$ (MM310) or $10^2$ copies $\mu g^{-1}$ (MM308) (Fig. 3). These results show that virus infections in various tissues were amplified from 6 to 13 days p.i. and then decreased, but virus remained detectable in each tissue until 27 days p.i.

## Detection of infectious virus in various tissues early after intrarectal infection

Although proviral DNA was present in each tissue early after infection, it was not clear whether these tissues released infectious virus. To observe the release of infectious virus from various tissues, infectious virus only was quantified in these tissues by using an infectious plaque assay. Infectious virus was first detected at 6 days p.i. in inguinal and mesenteric lymph nodes of two monkeys (MM300 and MM309) at 1·0 and 0·5 p.f.u. per $10^6$ cells, respectively (Fig. 4). Thereafter, the levels of infectious virus increased dramatically and high titres of infectious virus were detected in many lymphoid tissues of monkeys examined at 13 days p.i. (MM313 and MM334) (Fig. 4). In both of these monkeys, the highest numbers of infectious virus (119 and 100 p.f.u. per $10^6$ cells, respectively) were detected in the mesenteric lymph nodes, suggesting that this is the main site of production of infectious virus. Levels of infectious virus in the axillary and inguinal lymph nodes of these monkeys were 55·5–100·0 p.f.u. per $10^6$ cells. In MM313, levels of infectious virus in PBMCs and thymus (99·5 and 110·0 p.f.u. per $10^6$ cells, respectively) were almost as high as those in the mesenteric lymph node. However, MM334 tissues had remarkably low numbers of infectious virus in PBMCs and thymus (24·0 and 3·5 p.f.u. per $10^6$ cells, respectively). In the monkeys examined at 27 days p.i. (MM308 and MM310), infectious virus was detected at very low levels in lymphoid tissues ($<19$ p.f.u. per $10^6$ cells) (Fig. 4), whereas proviral DNA was detected at the same levels as at 13 days p.i. (Fig. 3). These results suggest that, after the peak of viraemia, high levels of virus existed in the lymphoid tissues, but most virus did not replicate there. In particular, PBMCs and thymus contained infectious virus at only 0–5 p.f.u. per $10^6$ cells at 27 days p.i., suggesting that these tissues hardly contribute to the release of infectious virus after the peak of viraemia.

In the intestinal tract, infectious virus was hardly detected throughout the infection (Fig. 4). At 13 days p.i., some infectious virus was detected in the jejunum, but titres were much lower than those in the lymphoid tissues (4·5 and 12·5 p.f.u. per $10^6$ cells in the jejuna of MM313 and MM334, respectively). These results show that virus replication was much lower in the intestinal tract than in the lymphoid tissues at the early phase of infection, although the virus reached the intestinal tract at the same time that it reached the lymphoid tissues.

## Sequential changes in the proportion of CD4$^+$ T cells in various tissues early after intrarectal infection

CD4$^+$ T cells have been reported as the main target and source for amplification of the virus. To estimate the effect of virus replication on the proportion of CD4$^+$ T cells existing in various tissues, sequential changes in the

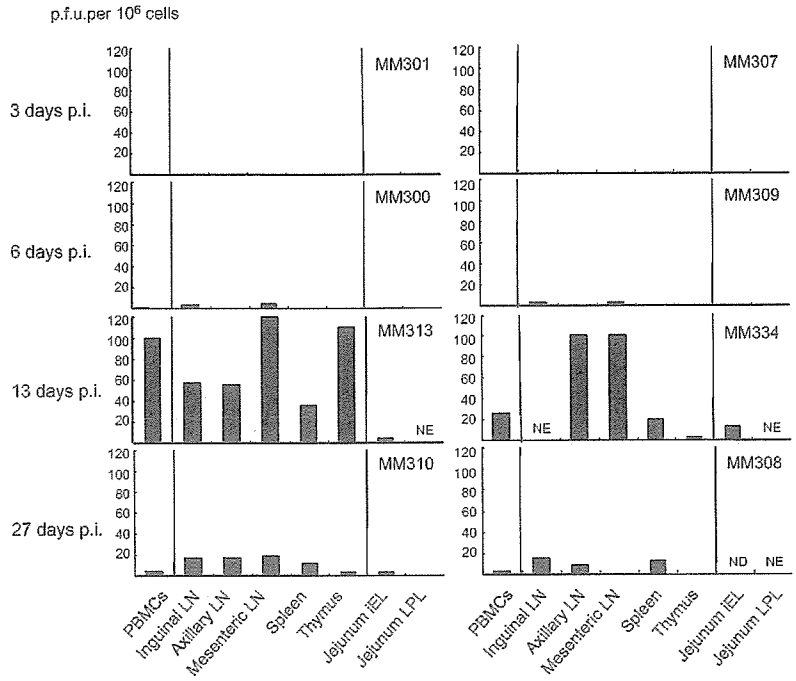


**Fig. 4.** Infectious virus loads in various tissues of eight SHIV-C2/1-KS661c-inoculated monkeys. Virus loads were determined by infectious plaque assay and are expressed as p.f.u. per $10^6$ cells. ND, Assay was not done because not enough lymphocytes were obtained; NE, culture was not evaluated because of contamination.

proportion of $CD4^+$ T cells were examined in each tissue in which virus was detected at various loads by using flow cytometry. The mean percentages of $CD4^+$ T cells in PBMCs, spleen, thymus, and inguinal, axillary and mesenteric lymph nodes of uninfected controls (MM244 and MM314) were 35, 26, 43, 59, 56 and 58 % of total lymphocytes, respectively (Fig. 5). The percentages of $CD4^+$ T cells in PBMCs were higher in monkeys at 6 and 13 days p.i. (62 and 61 % of total lymphocytes, respectively) than in the uninfected normal controls, but then decreased to 12 % of total lymphocytes by 27 days p.i. In other lymphoid tissues, the percentages of $CD4^+$ T cells remained at the level of uninfected normal controls until 6 days p.i. Between 6 and 27 days p.i., the percentages of $CD4^+$ T cells decreased significantly to 9–14 % of whole lymphocytes in each tissue.

In uninfected controls (MM244 and MM314), the percentages of $CD4^+$ T cells in the intestinal tract were lower than those in the lymphoid tissues. iEL and LPL were examined separately, because it was previously reported that the proportions of the major intestinal T-cell subsets differed markedly between the iEL and LPL (Veazey *et al.*, 1997, 2000a, b) and it was expected in the present study that the infection kinetics in iEL and LPL would differ. The mean percentages of $CD4^+$ T cells in the jejuna of control monkeys were 10 % in iEL and 34 % in LPL, and those in the rectums were 5 % in iEL and 11 % in LPL (Fig. 5). $CD4^+$ T cells in the intestinal tract remained at the same level as those in the uninfected controls until 13 days p.i. and then decreased to 1–2 % of whole lymphocytes by 27 days p.i. These sequential changes of $CD4^+$ T cells were almost the same in iEL and LPL of the jejunum and rectum. Thus, SHIV-C2/1 caused marked $CD4^+$ T-cell depletion both in peripheral blood and the intestinal tract. The extent of $CD4^+$ T-cell depletion in intestinal tract and lymphoid tissues correlated with the extent of virus replication in each tissue.

## Sequential changes in the proportion of CD4 single-positive (SP) and CD4CD8 double-positive (DP) T cells in the jejunum and thymus

There were larger percentages of CD4CD8 DP T cells in the jejunum than in the lymphoid tissues, apart from the thymus. In the jejuna of the normal control monkeys, the mean percentages of CD4CD8 DP T cells in total $CD4^+$ T cells were 64 % in iEL and 45 % in LPL, whereas in the lymphoid tissues, they were only 8–16 % (data not shown). The proportion of CD4 SP T cells in the jejunum remained at the level of uninfected controls until 13 days p.i. (15 and 34 % in jejunum iEL and LPL, respectively, at 13 days) and then dropped sharply to $<0{\cdot}3$ % in both iEL and LPL by 27 days p.i. This sequential change in the proportion of CD4 SP T cells in the jejunum was the same as that observed for total $CD4^+$ T cells. However, the proportion of CD4CD8 DP T cells started to decrease from day 3 p.i.; at 13 days p.i., it was $<5$ % in both iEL and LPL of the jejunum (Fig. 6).

In the thymus of the uninfected control monkeys, 91 % of $CD4^+$ T cells were CD4CD8 DP T cells (40 % of total lymphocytes). Moreover, the thymus had many CD3-negative ($CD3^-$) CD4CD8 DP cells (45 % of total lymphocytes). In the thymus, $CD3^+$ CD4CD8 DP cells tended to become depleted first, followed by $CD3^+$ CD4 SP cells and then $CD3^-$ CD4CD8 DP cells (Fig. 7). These results